Journal of Asian Earth Sciences 113 (2015) 238–253

Contents lists available at ScienceDirect

Journal of Asian Earth Sciences

journal homepage: www.elsevier.com/locate/jseaes

Two episodes of Late Paleozoic A-type magmatism in the Qunjisayi area, western Tianshan: Petrogenesis and tectonic implications

Ning-Bo Li [a,b], He-Cai Niu [a,c,*], Qiang Shan [a,c], Wu-Bin Yang [a,c]

[a] Key Laboratory of Mineralogy and Metallogeny, Guangzhou Institute of Geochemistry, Chinese Academy of Sciences, Guangzhou 510640, China
[b] University of Chinese Academy of Sciences, Beijing 100049, China
[c] Guangdong Provincial Key Laboratory of Mineral Physics and Materials, Guangzhou 510640, China

ARTICLE INFO

Article history:
Received 7 September 2014
Received in revised form 6 December 2014
Accepted 31 December 2014
Available online 7 January 2015

Keywords:
A-type granite
Mantle upwelling
Subduction roll-back
Western Tianshan
Central Asian Orogenic Belt (CAOB)

ABSTRACT

A-type magmatism is an effective lithoprobe for constraining the tectonic evolution of orogenic belts. In this study, we have identified two episodes of Late Paleozoic A-type magmatism in Qunjisayi, western Tianshan. Zircon U–Pb geochronology has yielded Late Carboniferous (rhyolites, 306 ± 2 Ma)- and Early Permian (granites, 296 ± 3 Ma) ages. Both the Qunjisayi rhyolites and granites have depleted Sr–Nd–Hf isotopic compositions, moderate A/CNK ratios (0.91–1) and negative Nb and Ta anomalies. They are also characterized by high $K_2O + Na_2O$ (8.72–10.6 wt.%), $FeO^T/(FeO^T + MgO)$ (0.86–0.99) and Y/Nb (1.42–2.34) values, similar to those of typical A_2-type granitoids. The Qunjisayi rhyolites may have been formed by partial melting of a juvenile calc-alkaline granitic crustal source induced by subduction roll-back in shallow depth. The succeeding Qunjisayi granites were likely to be derived from a lower crustal source that contains depleted mantle-derived components. Asthenospheric mantle upwelling, triggered by post-subduction slab break off, may have been important in the Qunjisayi granites formation. We conclude that the Late Paleozoic Qunjisayi A-type magmatism was genetically linked to the geodynamic transformation from late subduction to collision.

1. Introduction

Since the proposal of "A-type granite" (Loiselle and Wones, 1979), numerous hypotheses have been proposed on its petrogenesis, source characteristics and tectonic settings (Collins et al., 1982; Whalen et al., 1987; Creaser et al., 1991; Patiño Douce, 1997; Wu et al., 2002; Dall'Agnol et al., 2005, 2012; Agnol and de Oliveira, 2007; Bonin, 2007; Frost and Frost, 2011; Huang et al., 2011). The original definition of A-type granite was specific and included three diagnostic characteristics, namely being anhydrous, alkaline and anorogenic (Loiselle and Wones, 1979). Nevertheless, the term has subsequently been expanded to include a much broader spectrum of granites (Dall'Agnol et al., 2012). Hydrous and peraluminous/metaluminous members of A-type granites have been proposed by succeeding studies (e.g., Collins et al., 1982; Jung et al., 1998; Bi et al., 2000; Agnol and de Oliveira, 2007; Bonin, 2007). In addition, its exclusively anorogenic tectonic origin has also been challenged (e.g., Whalen et al., 1987; Eby, 1992; Espinoza et al., 2008; Shen et al., 2011; Li et al., 2012a).

A-type granite often coexists temporally and spatially with mafic magmatism (Peccerillo et al., 2003; Pirajno et al., 2008; Barboni and Bussy, 2013) and has high formation temperature (Wnrrn, 1986; Patiño Douce, 1997; King et al., 1997; Bonin, 2007), suggesting substantial involvement of mantle components (materials and/or heat) in its formation (e.g., Patiño Douce, 1997; Wu et al., 2002; Bonin, 2007; Li et al., 2012a; Qu et al., 2012). In addition, A-type granite is generally formed in tectonic settings that facilitate mantle upwelling, such as post-collisional or anorogenic extension (Whalen et al., 1987; Eby, 1990, 1992; Peccerillo et al., 2003; Dall'Agnol et al., 2005; Bonin, 2007; Moghazi et al., 2011), and subduction-related extensional settings (Espinoza et al., 2008; Zhao et al., 2008a; Shen et al., 2011; Li et al., 2012a). Therefore, a synthetic study on A-type granite provides significant information for revealing crust–mantle interaction and constraining regional tectonic evolution.

The Central Asian Orogenic Belt (CAOB) is the largest accretionary orogenic belt in the world (Sengor et al., 1993; Windley et al., 2007; Cawood et al., 2009; Xiao et al., 2009, 2010, 2013). More than 50% of the CAOB crust is juvenile (Kroner et al., 2014) and formed mainly during the Palaeozoic–Mesozoic (Sengor et al., 1993; Jahn et al., 2000; Jahn, 2004; Wilhem et al., 2012). At this period, voluminous granitoids and their volcanic equivalents, characterized by low initial Sr isotopic ratios and positive $\varepsilon_{Nd}(t)$ values, were formed

* Corresponding author at: Key Laboratory of Mineralogy and Metallogeny, Guangzhou Institute of Geochemistry, Chinese Academy of Sciences, Guangzhou 510640, China. Fax: +86 20 85290130.
E-mail address: niuhc@gig.ac.cn (H.-C. Niu).

http://dx.doi.org/10.1016/j.jseaes.2014.12.015
1367-9120/

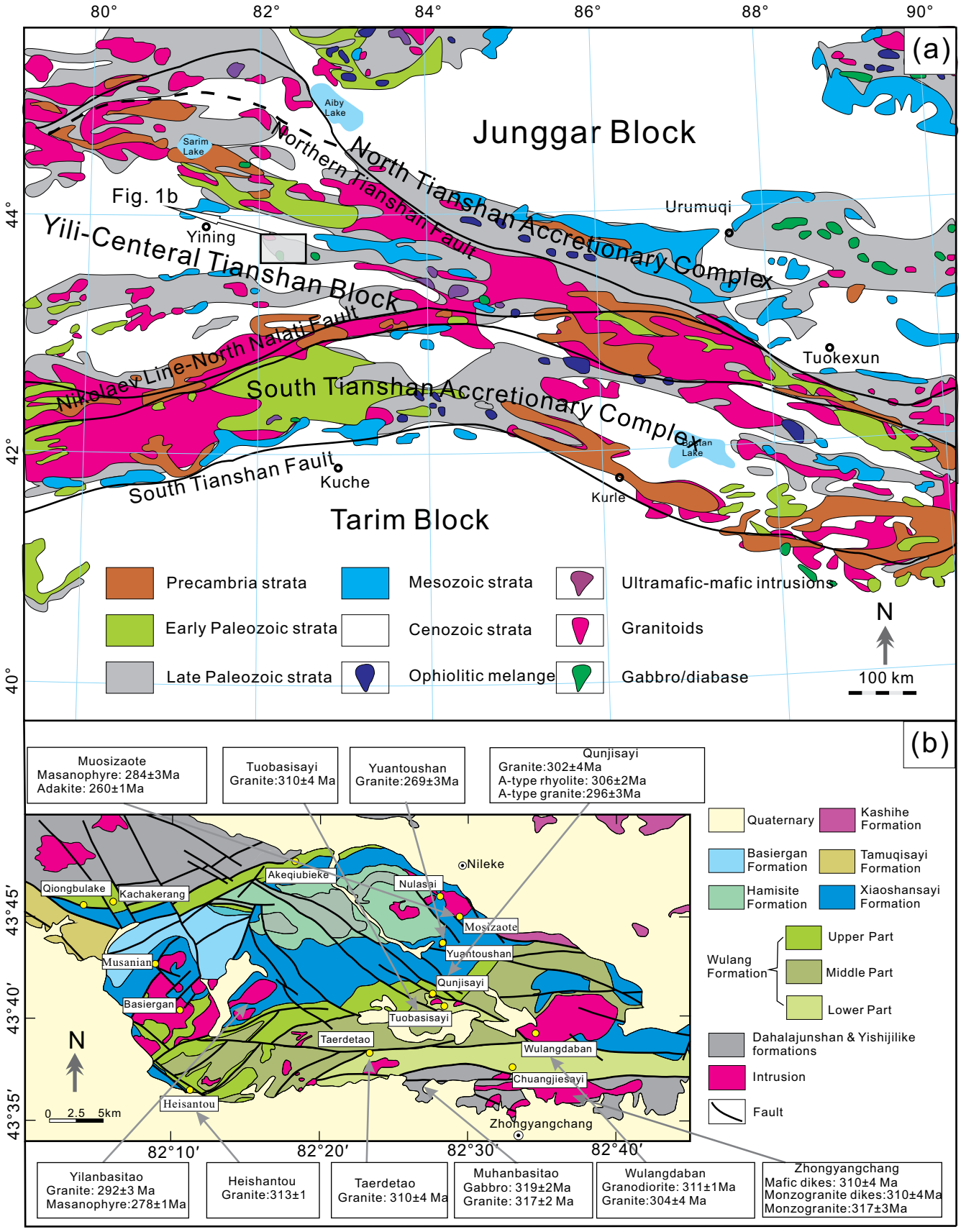

Fig. 1. (a) Geological map of western Tianshan (modified from Gao et al., 2009); (b) geological map of the western Awulale Mountain (modified from Li et al., 2013).

in the CAOB (Jahn et al., 2000; Jahn, 2004; Wu et al., 2002). Nevertheless, the petrogenesis and tectonic settings of these granitoids and their volcanic equivalents are still controversial. Western Tianshan is located in southwestern CAOB and formed by the amalgamation of the Tarim-, Yili–Central Tianshan- and Junggar blocks (Han et al., 2011; Long et al., 2011; Xiao et al., 2013), which makes it a critical region for studying the CAOB geodynamic evolution.

In this contribution, we present whole-rock elemental and Sr–Nd isotopic data, zircon U–Pb ages and Hf isotopic compositions of the two Late Paleozoic A-type felsic magmatic episodes in Qunjisayi area, western Tianshan. We attempt to better understand the petrogenesis of A-type granites and constrain the geodynamic evolution of the western Tianshan.

2. Local geology and petrology

Western Tianshan includes three major tectonic units, namely the South Tianshan Accretionary Complex (STAC), Yili–Central Tianshan Block (YCTB) and North Tianshan Accretionary Complex (NTAC) (Fig. 1a; Gao et al., 2009; Han et al., 2011; Xiao et al., 2013). It has experienced a long and complex evolutionary history, including Paleozoic subduction and collision events (Gao et al., 1998; Windley et al., 2007; Qian et al., 2009) and the Cenozoic reactivation as a consequence of the India–Eurasia collision (Hendrix et al., 1994; Sobel et al., 2006; Lu et al., 2013). The Devonian–Carboniferous STAC separates the Tarim Block from the YCTB (Fig. 1a), and was formed by the closure of the South Tianshan Ocean (Gao et al., 2009; Qian et al., 2009; Jiang et al., 2014). The YCTB is composed of Precambrian crystalline basement (Lei et al., 2011; Ma et al., 2012) and the overlying Paleozoic igneous rocks (Xia et al., 2004; Zhu et al., 2005; Zhu et al., 2006a, 2006b, 2009). The tectonic origin of the YCTB, i.e., whether it is part of the Tarim block (Lei et al., 2011; Ma et al., 2012) or an independent block (Liu et al., 2004; Lu et al., 2008), is still under debate. The NTAC is the main tectonic unit in the northern edge of western Tianshan and is sandwiched between the Junggar block to the north and the YCTB to the south (Fig. 1a). The accretionary complex formed by the closure of the North Tianshan Ocean (Jahn et al., 2000; Windley et al., 2007; Xiao et al., 2009, 2013; An et al., 2013).

Table 1
Compilation of geochronological data of Late Carboniferous to Permian igneous rocks in the western Awulale Mountain.

Localities	Rock types	Zircon U–Pb age (Ma)	References
Muhanbasitao	Gabbro	319 ± 2	Liu et al. (2012)
Zhongyangchang	Monzogranite	317 ± 3	Tang et al. (2014)
Muhanbasitao	Granite	317 ± 2	Lu et al. (2013)
Heishantou	Granite	313 ± 1	Zhao (2013)
Wulangdaban	Granodiorite	311 ± 1	Zhao (2013)
Zhongyangchang	Mafic dike	310 ± 4	Tang et al. (2014)
Zhongyangchang	Monzogranite dike	310 ± 4	Tang et al. (2014)
Taerdetao	Granite	310 ± 4	Author's unpublished data
Qunjisayi	A-type rhyolites	306 ± 2	This study
Wulangdaban	Granite	304 ± 4	Li et al. (2013)
Qunjisayi	Granite	302 ± 4	Yan et al. (2013)
Qunjisayi	A-type granites	296 ± 3	This study
Tuobasisayi	Granite	294 ± 3	Author's unpublished data
Yilanbasitao	Granite	292 ± 4	Li et al. (2012b)
Muosizaote	Masanophyre	284 ± 3	Zhao (2013)
Yilanbasitao	Masanophyre	278 ± 1	Zhao (2013)
Yuantoushan	Granite	269 ± 3	Li et al. (2013)
Muosizaote	Adakite	260 ± 1	Zhao et al. (2008b)

In central western Tianshan, the E-W trending Awulale Mountain is located in the eastern YCTB (Fig. 1a). The mountain comprises mainly Late Paleozoic igneous rocks (Zhu et al., 2005, 2006a,b; Yang et al., 2012) and contains numerous Fe–Cu deposits (Zhang et al., 2012b). The eastern part of the Awulale Mountain contains mainly Carboniferous basaltic rocks and the associated Fe deposits, whereas the western part contains Permian felsic rocks and the associated Cu deposits. The Qunjisayi felsic rocks are distributed in the western Awulale Mountain. Major structure in the region is the Qunjisayi syncline (ca. 50 km long and ca. 30 km

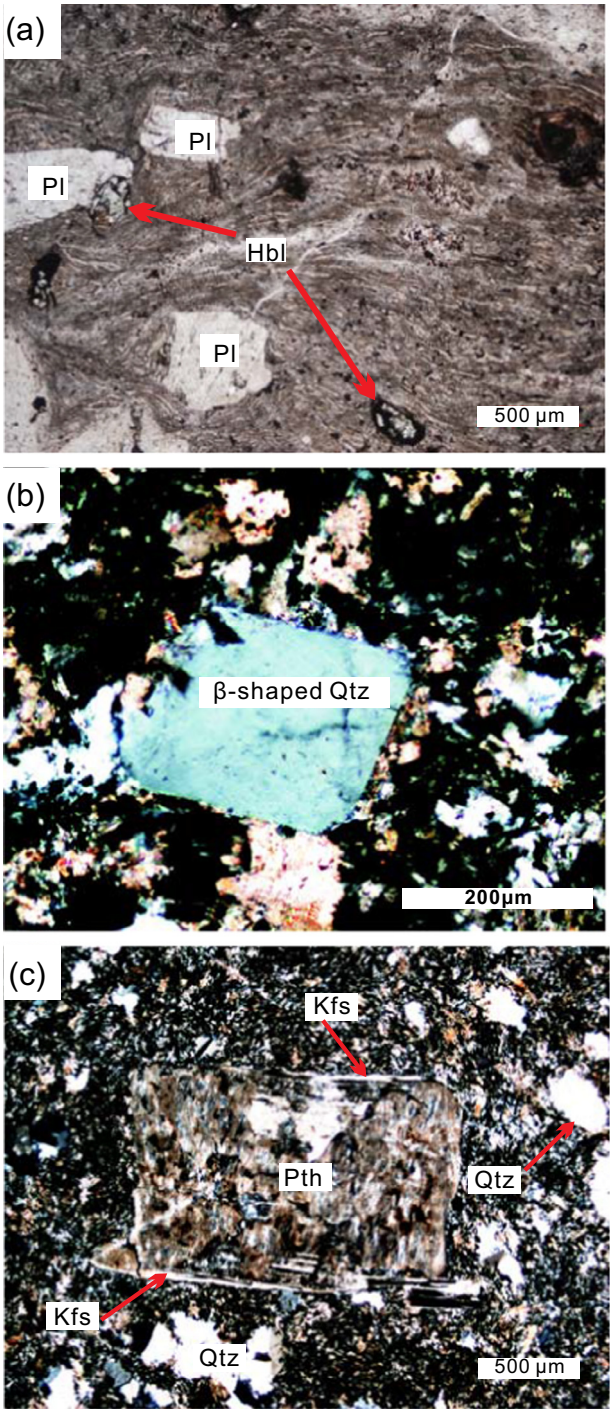

Fig. 2. Microphotographs of the Qunjisayi A-type felsic rocks. (a) Plagioclase and hornblende phenocrysts and the flow-banding of the Qunjisayi rhyolites; (b) quartz and (c) perthitic feldspar phenocrysts of the Qunjisayi granites. (Pl: plagioclase, Hbl: hornblende, Qtz: quartz, Pth: perthitic feldspar, Kfs: K-feldspar).

Table 2
Zircon U–Pb dating results of the Qunjisayi A-type felsic rocks.

Sample spots	Th (ppm)	U (ppm)	Th/U	Isotopic ratios						Apparent ages (Ma)			
				$^{207}Pb/^{206}Pb$	1σ	$^{207}Pb/^{235}U$	1σ	$^{206}Pb/^{238}U$	1σ	$^{207}Pb/^{235}U$	1σ	$^{206}Pb/^{238}U$	1σ
11QJ3-1 (rhyolite)													
1	185	237	0.78	0.05429	0.00376	0.35262	0.02390	0.04820	0.00076	307	18	303	5
2	247	290	0.85	0.06118	0.00382	0.39975	0.02457	0.04823	0.00071	341	18	304	4
3	114	152	0.75	0.05494	0.00350	0.36249	0.02176	0.04893	0.00081	314	16	308	5
4	59	86	0.68	0.05320	0.00689	0.33161	0.04000	0.04828	0.00111	291	31	304	7
5	125	145	0.86	0.05553	0.00383	0.36643	0.02350	0.04960	0.00079	317	17	312	5
6	61	95	0.64	0.05691	0.00492	0.36096	0.02651	0.04865	0.00102	313	20	306	6
7	351	380	0.92	0.05354	0.00260	0.35211	0.01756	0.04756	0.00078	306	13	300	5
8	231	270	0.86	0.04997	0.00247	0.33371	0.01607	0.04850	0.00068	292	12	305	4
9	50	83	0.60	0.05723	0.00497	0.36846	0.02954	0.04803	0.00104	319	22	302	6
10	108	116	0.93	0.05596	0.00528	0.37704	0.03426	0.04843	0.00095	325	25	305	6
11	96	116	0.82	0.05913	0.00419	0.39108	0.02511	0.04975	0.00096	335	18	313	6
12	247	290	0.85	0.06118	0.00382	0.39975	0.02457	0.04823	0.00071	341	18	304	4
13	198	180	1.10	0.05515	0.00369	0.36010	0.01977	0.04861	0.00084	312	15	306	5
14	102	130	0.78	0.05899	0.00513	0.39272	0.03170	0.04897	0.00088	336	23	308	5
15	94	144	0.65	0.05783	0.00387	0.38580	0.02478	0.04889	0.00087	331	18	308	5
16	219	283	0.77	0.05912	0.00312	0.39503	0.02007	0.04899	0.00082	338	15	308	5
17	61	87	0.70	0.05637	0.00473	0.36172	0.02760	0.04869	0.00107	313	21	307	7
18	114	152	0.75	0.05494	0.00350	0.36249	0.02176	0.04893	0.00081	314	16	308	5
19	59	86	0.68	0.05320	0.00689	0.33161	0.04000	0.04828	0.00111	291	31	304	7
20	125	145	0.86	0.05553	0.00383	0.36643	0.02350	0.04960	0.00079	317	17	312	5
21	61	95	0.64	0.05691	0.00492	0.36096	0.02651	0.04865	0.00102	313	20	306	6
10QJ-3D (granite)													
1	101	95	1.07	0.06294	0.00585	0.40225	0.03477	0.04823	0.00091	343	25	304	6
2	73	82	0.89	0.06867	0.00504	0.44029	0.03087	0.04711	0.00096	370	22	297	6
3	33	52	0.63	0.06552	0.00525	0.43380	0.03587	0.04747	0.00114	366	25	299	7
4	63	79	0.80	0.06046	0.00469	0.38129	0.02824	0.04655	0.00099	328	21	293	6
5	52	66	0.79	0.06593	0.00511	0.43707	0.03581	0.04797	0.00105	368	25	302	6
6	82	94	0.88	0.05755	0.00375	0.36696	0.02428	0.04628	0.00088	317	18	292	5
7	73	93	0.78	0.05279	0.00387	0.33043	0.02233	0.04697	0.00083	290	17	296	5
8	72	83	0.87	0.06108	0.00461	0.38647	0.02825	0.04631	0.00096	332	21	292	6
9	96	110	0.87	0.05326	0.00342	0.34695	0.02193	0.04713	0.00078	302	17	297	5
10	116	117	0.99	0.05104	0.00351	0.32877	0.02206	0.04655	0.00079	289	17	293	5
11	62	79	0.78	0.06563	0.00466	0.42747	0.03032	0.04807	0.00086	361	22	303	5
12	76	90	0.85	0.06583	0.00468	0.41418	0.02876	0.04600	0.00085	352	21	290	5
13	64	79	0.80	0.06498	0.00453	0.40480	0.02800	0.04592	0.00102	345	20	289	6
14	138	145	0.95	0.05423	0.00382	0.34992	0.02366	0.04745	0.00072	305	18	299	4
15	142	151	0.94	0.05171	0.00310	0.33332	0.01980	0.04681	0.00071	292	15	295	4
16	68	79	0.85	0.06258	0.00463	0.40678	0.02795	0.04782	0.00089	347	20	301	5
17	76	83	0.93	0.07300	0.00431	0.45770	0.02602	0.04629	0.00099	383	18	292	6

wide) (Fig. 1b). Strata outcropped in the region include the Carboniferous Yishijilike- and Dahalajunshan formations, the Permian Wulang-, Xiaoshansayi-, Hamisite-, Hamuqisa- and Basiergan formations and the Mesozoic Keshihe Formation (Fig. 1b). The Qunjisayi felsic rocks include rhyolites hosted by the Wulang Formation (to be described below) and granites intruded into it. The Wulang Formation in Qunjisayi comprises three parts: the lower part is dominated by basalt, dacite and rhyolite; the overlying middle part shares similar rock types with those of the lower part, whereas the upper part is composed of a volcanic suite (e.g., tuff, rhyolite and porphyritic basalt) with minor sandstone. The age of this formation is not well-constrained: some intrusions in the Wulang Formation have yielded Carboniferous zircon U–Pb ages, such as the Qunjisayi granite porphyry (302 Ma) (Yan et al., 2013) and Taerdetao granite (310 Ma) (Author's unpublished data). Intrusive rocks in the western Awulale Mountain, including granitoids, gabbro and adakite, are mainly formed in ca. 320–260 Ma (Fig. 1b and Table 1).

The Qunjisayi rhyolites are characterized by porphyritic and flow textures, with phenocrysts of plagioclase (5–10 vol.%), K-feldspar (25–30 vol.%), quartz (35–45 vol.%) and minor hornblende (Fig. 2a) The Qunjisayi granites are pink and have porphyritic texture, with phenocrysts of quartz (35–40 vol.%), albite (35–45 vol.%) and perthite (15–20 vol.%) with minor accessory minerals (e.g., magnetite and apatite), The A-type granites also contain some minerals with special textures, such as the β-shaped quartz (Fig. 2b) and perthitic cores with K-feldspar rims (Fig. 2c).

3. Analytical methods

Zircon separation was carried out using conventional density and magnetic separation techniques to concentrate non-magnetic heavy fractions. Representative zircon grains were then hand-picked under a binocular microscope and mounted in epoxy mounts, which were then polished to nearly half-section to expose their internal structures. All mounted zircon grains were studied petrographically with transmitted- and reflected light microscopy, as well as by cathodoluminescence (CL) imaging to reveal their internal structures. Zircon U–Pb dating of the Qunjisayi rhyolites was performed on a laser ablation inductively coupled plasma spectrometry (LA-ICPMS) at the State Key Laboratory of Continental Dynamics of the Northwest University, China. Standard zircon 91500 was used as the external standard for calibration (Wiedenbeck et al., 1995). The analytical procedures were described by Yuan et al. (2004). Zircon U–Pb dating of Qunjisayi granites was carried out on an Agilent 7500a LA-ICPMS at the State Key Laboratory of Isotope Geochemistry, Guangzhou Institute of Geochemistry, Chinese Academy of Sciences (GIGCAS). Standard zircon TEM was used as the external standard for calibration (Black et al., 2004). Details on the LA-ICPMS operating conditions were described by Tu et al. (2011) and Li et al. (2012a). Both isotope ratios and trace elements contents of zircon were calculated using ICPMSDataCal 9.0 (Liu et al., 2008, 2010). The analytical data were calculated and plotted using Isoplot 4.11 (Ludwig, 2008).

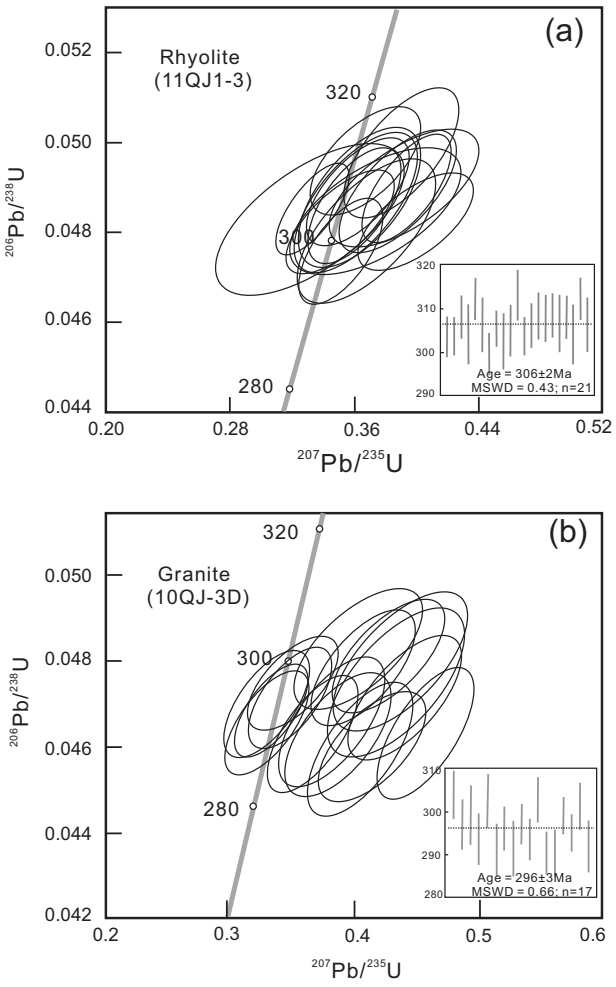

Fig. 3. Concordia diagrams of LA-ICP-MS zircon U–Pb analyses for the Qunjisayi A-type felsic rocks.

Zircon Hf isotopic analyses were determined by a Nu Plasma MC-ICPMS, equipped with GeoLas 2005 excimer ArF laser-ablation system, at the State Key Laboratory of Continental Dynamics of the Northwest University. Zircon 91500 was used as the external standard and was analyzed once every five analyses. The analytical procedures were described by Yuan et al. (2008).

Whole rock major elements were analyzed by standard X-ray fluorescence (XRF) methods as outlined by Li et al. (2005) at the GIGCAS. Trace elements were determined at the GIGCAS by using the Perkin–Elmer ELAN 6000 ICPMS following procedures described by Li (1997), with less than 5% of standard deviations for most elements. Sr and Nd isotopic compositions were determined by using a Neptune Plus MC-ICPMS at the GIGCAS, using analytical procedures described by Wei et al. (2002) and Liang et al. (2003). The mass fractionation corrections for Sr and Nd isotopic ratios are based on $^{86}Sr/^{88}Sr$ ratio of 0.1194 and $^{146}Nd/^{144}Nd$ ratio of 0.7219, respectively. The $^{87}Sr/^{86}Sr$ ratio of the Standard NBS SRM 987 and the $^{143}Nd/^{144}Nd$ ratio of the Standard Shin Etsu JNdi-1 determined during this study were 0.71025 and 0.512115, respectively.

4. Results

4.1. Zircon U–Pb and Hf isotopic analyses

Zircon grains from Qunjisayi felsic rocks were U–Pb dated (Table 2; Fig. 3). Zircon grains in the Qunjisayi rhyolite (11QJ1-3) are ca. 60–150 μm long with length/width ratios of 1:1–4:1. The zircon grains show obvious oscillatory zonation in CL images and commonly contain melt inclusions. These characteristics, together with their relatively high Th/U ratios (0.60–1.10) (Table 2), indicate that the zircon grains from the Qunjisayi rhyolites are magmatic (Belousova et al., 2002; Yang et al., 2014b). 21 Zircon grains have given $^{206}Pb/^{238}U$ ages of ca. 300–313 Ma (Table 2). The ages plot on or near concordia with a weighted mean $^{206}Pb/^{238}U$ age of 306 ± 2 Ma (MSWD = 0.43) (Fig. 3a). Zircon grains in the Qunjisayi granite (10QJ-3D) are 50–150 μm long with length/width ratios of 1:1–2:1. They are also magmatic owing to they have obvious oscillatory zonation, melt inclusions and high Th/U ratios (0.63–1.07) (Table 2). 17 Analyses give $^{206}Pb/^{238}U$ ages of ca. 289–304 Ma (Table 2) and a weighted mean $^{206}Pb/^{238}U$ age of 296 ± 3 Ma (MSWD = 0.66) (Fig. 3b).

The Qunjisayi rhyolites have zircon $\varepsilon_{Hf}(t)$ values ranging from +7.1 to +14 (Avg. = +10.8) and T_{DM} (Hf) model ages of 425–869 Ma (Avg. = 630 Ma) (Table 3). The Qunjisayi granites have zircon $\varepsilon_{Hf}(t)$ values ranging from +9 to +16 (Avg. = +13.1) and T_{DM} (Hf) model ages of 292–738 Ma (Avg. = 472 Ma) (Table 3).

4.2. Whole rock major and trace elements

The Qunjisayi rhyolites have high contents of SiO_2 (70.9–72.5 wt.%) and total alkali (9.31–10.6 wt.%), and their K_2O/Na_2O ratios vary from 1.52 to 3.55 (Table 4). All rhyolite samples plot in the shoshonite field on the K_2O vs. SiO_2 diagram (Fig. 4a). They have A/CNK values ranging from 0.94 to 0.99, indicating their metaluminous nature (Fig. 4b). The rhyolites contain low MgO (0.22–0.3 wt.%), CaO (0.39–1.13 wt.%), TiO_2 (0.36–0.42 wt.%) and P_2O_5 (0.04–0.05 wt.%) contents but relatively high $Fe_2O_3^T$ (2.5–2.87 wt.%) and Al_2O_3 (12.97–13.4 wt.%) contents. On the primitive-mantle normalized multi-element diagram, the rhyolites show negative Ba, Sr, Nb and Ta anomalies and positive Zr and Hf anomalies (Fig. 5a). They have similar chondrite-normalized REE patterns, which are enriched in light rare earth elements (LREEs) ($(La/Yb)_N$ = 3.21–5.76), display negative Eu anomalies (Avg. Eu/Eu^* = 0.35) (Fig. 5b), and have nearly flat heavy rare earth element (HREE) patterns ($(Tb/Yb)_N$ = 0.78–0.97).

The Qunjisayi granites have also high SiO_2 (69.9–72.11 wt.%) and total alkali (8.72–9.78 wt.%) contents (Table 4). They have lower K_2O (2.53–4.67 wt.%) contents but higher TiO_2 (0.4–0.57 wt.%), Al_2O_3 (13.32–15.34 wt.%), Na_2O (4.69–7.25 wt.%) and P_2O_5 (0.05–0.06 wt.%) contents than those of the Qunjisayi rhyolites (Fig. 6a–e). All the Qunjisayi granites plot in the middle- to high-*K* calc-alkaline field on the K_2O vs. SiO_2 diagram, with K_2O/Na_2O ratios ranging from 0.35 to 0.95 (Fig. 4a). They also display metaluminous nature with A/CNK values ranging from 0.91 to 1(Fig. 4b). Although in the primitive-mantle normalized multi-element diagram the granite samples also show significant negative Ba, Sr, Nb and Ta anomalies and positive Zr, Hf anomalies (Fig. 5a), they have lower Ba and Rb but higher Zr and Hf contents than those of the Qunjisayi rhyolites (Fig. 6f–i). The granites also have flat HREE patterns ($(Tb/Yb)_N$ = 0.86–1.45), but are more enriched in LREEs ($(La/Yb)_N$ = 3.56–8.41) and have weaker Eu anomalies (Average Eu/Eu^* = 0.66) than the Qunjisayi rhyolites (Fig. 5b).

4.3. Sr–Nd isotopic compositions

The whole rock Sr–Nd isotopic data of the Qunjisayi felsic rocks are listed in Table 4. Whole rock $(^{87}Sr/^{86}Sr)_i$ and $\varepsilon_{Nd}(t)$ values have been calculated at 306 Ma for the Qunjisayi rhyolites and at 296 Ma for the Qunjisayi granites. The Qunjisayi rhyolites have consistent $\varepsilon_{Nd}(t)$ values ranging from +5.2 to +5.4 (Table 4). The Qunjisayi granites have a low and narrow range of initial $^{87}Sr/^{86}Sr$

Table 3
LA-MC-ICPMS zircon Lu–Hf isotope data for the Qunjisayi A-type felsic rocks.

Sample spots	$^{176}Yb/^{177}Hf$	$^{176}Lu/^{177}Hf$	$^{176}Hf/^{177}Hf$	2σ	Age (Ma)	$(^{176}Hf/^{177}Hf)_i$	$\varepsilon_{Hf}(t)$	2σ	T_{DM} (Ma)
11QJ3-1 (rhyolite)									
1	0.065055	0.001969	0.282849	0.000009	303	0.282837	9.0	0.6	745
2	0.060150	0.001640	0.282988	0.000020	304	0.282978	14.0	0.9	425
5	0.046127	0.001364	0.282848	0.000026	312	0.282840	9.3	1.1	732
6	0.051768	0.001413	0.282942	0.000019	306	0.282934	12.5	0.9	524
7	0.069462	0.001869	0.282926	0.000020	300	0.282916	11.7	0.9	569
8	0.093111	0.002665	0.282903	0.000022	305	0.282887	10.8	1.0	630
9	0.068700	0.001970	0.282838	0.000024	302	0.282827	8.6	1.0	769
10	0.066692	0.001767	0.282921	0.000020	305	0.282911	11.6	0.9	577
11	0.048982	0.001370	0.282859	0.000021	313	0.282851	9.7	0.9	707
12	0.081736	0.002195	0.282952	0.000021	304	0.282939	12.6	0.9	513
13	0.083861	0.002232	0.282929	0.000025	306	0.282916	11.8	1.1	565
15	0.042231	0.001093	0.282957	0.000021	308	0.282951	13.1	0.9	485
16	0.056713	0.001692	0.282790	0.000027	308	0.282781	7.1	1.1	869
17	0.062881	0.001812	0.282860	0.000029	307	0.282850	9.5	1.2	714
18	0.096893	0.002564	0.282908	0.000023	308	0.282893	11.1	1.0	615
19	0.062400	0.001702	0.282905	0.000017	304	0.282895	11.0	0.8	614
20	0.054256	0.001477	0.282883	0.000020	312	0.282874	10.5	0.9	656
10QJ-3D (granite)									
1	0.040318	0.001468	0.282931	0.000017	304	0.282923	12.0	0.8	551
2	0.043387	0.001568	0.282966	0.000015	297	0.282957	13.1	0.8	477
4	0.025606	0.000955	0.282915	0.000019	299	0.282910	11.5	0.9	583
5	0.040114	0.001486	0.282973	0.000022	293	0.282965	13.3	0.9	463
6	0.037161	0.001360	0.282955	0.000022	292	0.282948	12.6	0.9	501
7	0.042990	0.001544	0.282998	0.000020	296	0.282990	14.2	0.9	404
8	0.044489	0.001580	0.283041	0.000025	292	0.283032	15.6	1.0	309
9	0.042386	0.001540	0.283040	0.000016	297	0.283031	15.7	0.8	309
10	0.046144	0.001768	0.283045	0.000017	293	0.283036	15.8	0.8	301
11	0.038554	0.001427	0.283045	0.000018	303	0.283037	16.0	0.8	292
12	0.027566	0.000993	0.282897	0.000022	290	0.282891	10.6	0.9	631
13	0.035330	0.001311	0.282922	0.000021	289	0.282915	11.4	0.9	577
14	0.027863	0.001040	0.282847	0.000016	299	0.282842	9.0	0.8	738
15	0.027440	0.001062	0.282966	0.000025	295	0.282960	13.2	1.0	471

values from 0.7034 to 0.7052, with positive $\varepsilon_{Nd}(t)$ values varying from +3.8 to +4.3 (Table 4).

5. Discussion

5.1. A-type affinity

Typical A-type granitoids are characterized by enrichments of $Na_2O + K_2O$, HFSEs (e.g., Zr, Nb, Ga and Y) and REEs (except Eu) (Whalen et al., 1987). They also have high $FeO^T/(FeO^T + MgO)$ values (Fig. 7a), indicating that most of them are ferrous (Frost et al., 2001; Frost and Frost, 2011). Both the Qunjisayi rhyolites and granites have high $FeO^T/(FeO^T + MgO)$ values (0.86–0.99) and all plot in the A-type field in the A-type granitoid discrimination diagrams (Fig. 7; Frost et al., 2001; Frost and Frost, 2011). Another important feature of typical A-type granitoids is that they form commonly under high temperature, as demonstrated by their elevated HFSE contents (whose solubility in melts increase with temperature) (Watson, 1979; Collins et al., 1982) and the occasional presence of some ferromagnesian minerals (e.g., pyroxene) (King et al., 1997, 2001; Patiño Douce, 1999; Bonin, 2007; Jiang et al., 2009; Huang et al., 2011; Sun et al., 2011). Zircon saturation thermometry provides an effective way for estimating magmatic temperatures (Watson, 1979; Watson and Harrison, 1983). The zircon saturation temperatures of the Qunjisayi rhyolites vary from 859 °C to 884 °C and the granites vary from 863 °C to 906 °C, which are significantly higher than those of typical I-type granitoids (under 800 °C, King et al., 1997) but close to that of typical A-type granitoids (>870 °C, King et al., 1997). In addition, the Qunjisayi granites contain euhedral β-shaped quartz (Fig. 2b) and perthitic cores with K-feldspar rims (Fig. 2c), which are diagnostic minerals for A-type granitoids (Bonin, 2007). As a result, we conclude that the Qunjisayi felsic rocks belong to typical A-type series.

5.2. Petrogenesis

Petrogenesis of typical A-type granitoids is still controversial, and the major debates focus on their sources. Four main hypotheses have been previously proposed, including: (1) fractionation of mantle-derived alkali basaltic magmas with or without crustal contamination (e.g., Loiselle and Wones, 1979; Eby, 1990; Bonin, 2007); (2) anatexis of underplated calc-alkaline granitic crustal rocks in the shallow crust (e.g., Creaser et al., 1991; Patiño Douce, 1997); (3) low degree partial melting of lower-crustal granulite residues (from which granitic melts were previously extracted) (e.g., Collins et al., 1982; Clemens et al., 1986; Whalen et al., 1987; King et al., 1997); (4) partial melting of previous underplated basaltic rocks in the lower crust (e.g., Frost and Frost, 1997; Frost et al., 2001; Wu et al., 2002; Wang et al., 2010); and (5) high-temperature (>960 °C) melting of granulite-facies metasedimentary rocks (e.g., Huang et al., 2011; Sun et al., 2011). The first four hypotheses suggest igneous source rocks, whereas the last hypothesis proposes a metasedimentary one. Among these petrogenetic models, interaction of mantle-derived magma with crustal rocks and direct partial melting of crustal rocks are considered as the most important mechanism.

5.2.1. Qunjisayi rhyolites

Geochemical characteristics of the Qunjisayi rhyolites are inconsistent with the metasedimentary-melting petrogenetic model, because the rhyolites have low A/CNK values (Fig. 4b) and no aluminous minerals (e.g., muscovite; Chappell et al., 1987). In addition, the rhyolites have depleted Nd–Hf isotopic

Table 4
Major (wt.%) and trace elements (ppm) and Sr–Nd isotope compositions of Qunjisayi A-type felsic rocks.

Sample	Rhyolites						Granites	
	12QJ-9	12QJ-10	12QJ-12	11QJ1-1	11QJ1-3	11QJ1-4	QJ1-2	QJ1-3
SiO_2	71.01	72.43	71.72	71.58	72.5	70.94	72.11	71.71
TiO_2	0.39	0.37	0.42	0.39	0.38	0.36	0.52	0.53
Al_2O_3	13.40	13.16	13.08	13.10	13.20	12.97	13.8	14.13
$Fe_2O_3^T$	2.69	2.50	2.87	2.52	2.61	2.71	2.27	2.27
MnO	0.05	0.03	0.03	0.04	0.04	0.04	0.03	0.04
MgO	0.25	0.28	0.24	0.3	0.22	0.23	0.17	0.33
CaO	0.39	0.76	0.76	1.13	0.83	0.82	0.52	0.56
Na_2O	2.33	4.31	3.78	2.54	3.10	3.12	4.96	4.94
K_2O	8.27	5.07	5.76	7.05	6.48	6.19	4.37	4.67
P_2O_5	0.04	0.04	0.05	0.04	0.04	0.04	0.06	0.06
L.O.I	0.62	0.83	0.94	0.94	0.61	0.73	0.83	0.41
Total	99.54	99.84	99.73	99.63	100.01	98.15	99.64	99.65
Sc	6.42	5.63	6.21	6.01	5.18	4.89	6.72	6.60
V	17.9	30.7	20.5	24.6	22.1	20.8	24.3	20.5
Cr	21.8	21.2	26.6	29.8	23.2	24.2	0.17	0.57
Co	2.52	2.19	2.25	1.83	1.61	1.99	25.9	22.4
Ni	1.48	1.30	1.90	7.92	1.36	1.90	0.43	0.83
Zn	86.4	33.0	64.9	78.6	60.0	55.1	11.7	29.0
Ga	16.1	15.5	13.8	13.6	15.4	14.7	17.3	17.7
Ge	1.12	1.36	1.18	1.23	1.44	1.34	1.32	1.28
Rb	194	106	129	163	148	139	85.8	90.0
Sr	55.8	35.2	54.9	54.0	55.0	53.2	76.8	47.7
Y	30.0	37.1	38.5	34.0	33.6	31.3	34.4	34.4
Zr	44	399	413	458	489	451	582	552
Nb	18.7	17.9	17.5	16.3	18.9	17.7	20.0	20.1
Ba	935	579	641	956	723	687	612	506
La	29.2	26.2	26.8	21.8	37.7	27.9	51.0	40.4
Ce	62.0	65.1	61.8	49.2	77.5	58.4	105	85.9
Pr	7.53	8.27	8.04	6.21	8.80	7.11	13.6	11.4
Nd	29.1	30.7	31.6	23.7	30.5	25.8	49.1	42.1
Sm	5.68	6.44	6.41	4.83	5.22	4.93	8.54	7.81
Eu	0.54	0.68	0.63	0.70	0.54	0.51	1.55	1.43
Gd	4.90	5.93	6.12	4.73	4.63	4.23	6.57	6.12
Tb	0.85	1.06	1.03	0.86	0.85	0.81	1.13	1.04
Dy	5.56	6.78	6.83	5.67	5.53	5.14	6.77	6.67
Ho	1.27	1.52	1.59	1.33	1.31	1.21	1.42	1.40
Er	3.90	4.58	4.68	3.93	3.99	3.76	4.31	4.09
Tm	0.66	0.74	0.74	0.68	0.67	0.67	0.64	0.68
Yb	4.51	4.89	4.83	4.88	4.70	4.71	4.35	4.34
Lu	0.72	0.74	0.75	0.81	0.81	0.78	0.71	0.67
Hf	10.2	9.46	9.44	11.1	10.2	9.63	13.4	13.4
Ta	1.42	1.31	1.31	1.26	1.35	1.29	1.26	1.27
Pb	11.0	5.86	10.7	9.39	5.53	5.90	9.24	3.15
Th	18.6	17.4	16.7	17.8	17.5	16.7	15.8	15.3
U	4.42	4.60	4.06	4.95	4.56	4.52	5.30	3.71
T_{Zr}	875	859	862	873	884	876	904	897
$^{87}Rb/^{86}Sr$							3.237	5.471
$^{87}Sr/^{86}Sr$							0.718864	0.727628
2σ							0.000012	0.000011
$(^{87}Sr/^{86}Sr)_i$							0.705185	0.704506
$^{147}Sm/^{144}Nd$				0.123	0.104	0.115	0.105	0.112
$^{143}Nd/^{144}Nd$				0.512765	0.512724	0.512740	0.512659	0.512670
2σ				0.000003	0.000003	0.000003	0.000006	0.000006
$\varepsilon_{Nd}(t)$				5.4	5.3	5.2	3.9	3.8
$T_{DM.2}$ (Ma)				631	633	646	744	747

Samples	Granites							
	QJ1-4	QJ1-5	QJ1-6	QJ1-7	QJ2-4	11QJ5-1	11QJ5-2	10QJ-3D
SiO_2	71.6	70.9	70.62	69.9	71.37	71.51	70.17	70.06
TiO_2	0.52	0.52	0.55	0.57	0.54	0.4	0.44	0.49
Al_2O_3	14.32	14.21	15.1	15.34	14.14	13.32	14.23	14.33
$Fe_2O_3^T$	2.26	2.27	2.19	2.42	3.16	3.2	3.56	2.53
MnO	0.04	0.04	0.02	0.01	0.02	0.03	0.03	0.06
MgO	0.26	0.26	0.06	0.03	0.15	0.26	0.29	0.2
CaO	0.55	1.26	0.63	0.65	0.59	1.12	1.01	1.42
Na_2O	5.17	5.61	6.89	7.25	6.1	4.69	5.48	5.15
K_2O	4.48	3.67	2.71	2.53	2.85	4.03	3.65	4.32
P_2O_5	0.05	0.05	0.06	0.06	0.05	0.05	0.06	/
L.O.I	0.4	0.85	0.84	0.88	0.68	0.89	0.74	1.04
Total	99.65	99.64	99.67	99.64	99.65	99.49	99.66	99.6

Table 4 (*continued*)

Samples	Granites							
	QJ1-4	QJ1-5	QJ1-6	QJ1-7	QJ2-4	11QJ5-1	11QJ5-2	10QJ-3D
Sc	7.38	6.73	7.09	7.44	5.50	5.46	5.67	6.96
V	27.1	19.8	41.0	44.8	19.8	20.1	24.0	15.4
Cr	1.29	0.76	1.76	0.98	0.08	13.8	51.6	34.9
Co	24.5	14.7	28.3	13.5	26.8	2.23	3.24	1.33
Ni	0.12	0.86	0.49	0.28	0.61	1.24	2.78	1.01
Zn	26.3	25.0	3.04	0.73	4.81	23.4	30.3	34.3
Ga	17.9	17.6	20.3	21.7	16.8	15.5	16.6	16.2
Ge	1.42	1.21	1.04	1.13	1.25	1.27	1.63	1.33
Rb	89.6	66.1	48.3	44.3	52.6	89.4	76.9	86.2
Sr	62.1	51.6	47.5	48.6	40.9	57.6	70.4	53.3
Y	35.0	34.2	37.0	38.8	28.0	43.0	44.1	35.1
Zr	559	573	634	620	588	421	559	522
Nb	21.0	19.3	21.8	21.6	19.7	19.7	18.8	19.8
Ba	553	370	228	201	338	397	375	445
La	45.2	42.9	51.1	56.0	25.9	28.2	46.3	23.1
Ce	96.6	89.9	103	106	67.3	70.2	105	59.7
Pr	12.5	11.9	12.9	13.6	8.57	9.70	13.5	8.44
Nd	46.6	43.9	47.9	50.3	32.4	37.6	49.1	34.2
Sm	8.46	8.11	8.43	8.67	6.11	7.57	8.96	7.12
Eu	1.63	1.59	1.67	1.74	0.97	0.90	1.17	1.34
Gd	6.76	6.39	6.66	6.94	4.55	6.95	7.91	6.26
Tb	1.19	1.09	1.14	1.18	0.71	1.24	1.39	1.09
Dy	7.10	6.91	7.09	7.36	4.58	7.72	8.32	6.45
Ho	1.52	1.46	1.50	1.58	1.02	1.72	1.86	1.41
Er	4.33	4.11	4.53	4.47	3.27	5.04	5.16	3.98
Tm	0.68	0.66	0.72	0.71	0.52	0.82	0.86	0.63
Yb	4.73	4.38	4.54	4.80	3.77	5.67	5.62	4.36
Lu	0.73	0.70	0.77	0.76	0.63	0.91	0.90	0.68
Hf	13.6	13.8	14.8	14.0	13.1	9.50	11.8	10.3
Ta	1.41	1.23	1.37	1.28	1.20	1.44	1.38	1.25
Pb	3.14	2.52	3.29	5.76	9.10	6.45	10.8	7.63
Th	16.4	16.1	17.0	16.0	15.1	18.2	17.1	14.1
U	4.22	3.79	6.16	5.50	3.51	5.59	6.07	3.43
T_{Zr}	898	888	906	900	903	863	891	\
$^{87}Rb/^{86}Sr$	4.184	3.706	2.946	2.640				4.689
$^{87}Sr/^{86}Sr$	0.722891	0.720905	0.717548	0.716257				0.722863
2σ	0.000011	0.000014	0.000009	0.000013				0.000012
$(^{87}Sr/^{86}Sr)_i$	0.705206	0.705241	0.705097	0.705102				0.703048
$^{147}Sm/^{144}Nd$	0.110	0.112	0.106	0.104				0.126
$^{143}Nd/^{144}Nd$	0.512665	0.512670	0.512660	0.512662				0.512722
2σ	0.000006	0.000006	0.000007	0.000007				0.000004
$\varepsilon_{Nd}(t)$	3.8	3.8	3.9	4.0				4.3
$T_{DM.2}$ (Ma)	747	747	745	735				707

T_{Zr}: zircon saturation temperatures (°C), according to Watson and Harrison (1983).

composition (Tables 3 and 4; Fig. 8a and b). Furthermore, sedimentary rocks are rare and all the previously studied granitoids have igneous rock sources in Qunjisayi area (e.g., Li et al., 2013; Yan et al., 2013; Zhao, 2013; Tang et al., 2014). Direct partial melting of a mantle source cannot generate granitic magmas (Taylor and McLennan, 1985), whereas fractional crystallization of mantle-derived mafic melts can produce A-type granitic magmas (Eby, 1990; Turner et al., 1992; Bonin, 2007). Several lines of evidence argue against fractional crystallization as being important for generating the Qunjisayi rhyolites: (1) the rhyolites have low Rb/Sr (2.36–3.47), narrow range of SiO_2 contents (70.94–72.43 wt.%) and Eu/Eu* (0.31–0.45) values (Table 4), suggesting that fractional crystallization may have been minor; (2) magmatic rocks derived from fractional crystallization of mantle-derived mafic melts should exhibit a continuous compositional trend from mafic through intermediate to felsic rocks (Wang et al., 2010). However, intermediate igneous rocks have not been identified in the region. Although the "residual granulite melting" model can explain the lower water fugacity and high halogen content of some A-type granitoids, it cannot explain some geochemical characteristics (e.g., high $FeO^T/(FeO^T + MgO)$) of some A-type granitoids (Creaser et al., 1991; Frost and Frost, 1997; Wu et al., 2002). The Qunjisayi rhyolites have significantly high $FeO^T/(FeO^T + MgO)$ values (Fig. 7a), therefore, this residual model cannot explain the formation of the rhyolites. The Qunjisayi rhyolites have negative Eu, Ba and Sr anomalies (Fig. 5a and b), indicating that they may have been produced by partial melting a crustal source in the stability field of plagioclase (e.g., Wang et al., 2010). If plagioclase is the dominated residual phase in the source region, the K_2O/Na_2O ratios of melts could be elevated because plagioclase crystallization can remove Na_2O (Patiño Douce, 1997). According to experimental studies (Skjerlie and Johnston, 1993; Patiño Douce, 1997), dehydration melting of calc-alkaline granitoids in the shallow crust (at depths of 15 km or less) can produce A-type granitoids with unusual high K_2O/Na_2O ratios. The K_2O/Na_2O ratios (1.18–3.55) of the Qunjisayi rhyolites are similar to these of the A-type granitic melts produced by the previous experiments (1.59–2.18; Patiño Douce, 1997). Therefore, we favor the derivation of the rhyolites from direct partial melting of calc-alkaline granitic crustal rocks at a shallow depth. In addition, The Qunjisayi rhyolites have depleted Nd–Hf isotopic compositions and relatively young Nd (631–646 Ma) and Hf (426–886 Ma) model ages (Fig. 8a and b; Tables 3 and 4), implying that their source composed mainly of juvenile materials.

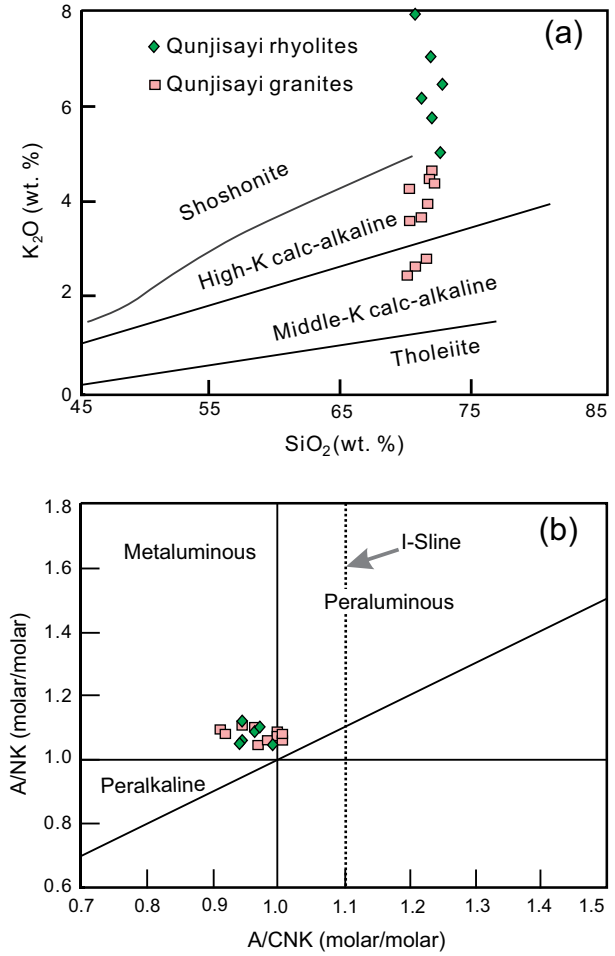

Fig. 4. (a) K_2O vs. SiO_2 and (b) A/NK vs. A/CNK geochemical discrimination diagrams for the Qunjisayi A-type felsic rocks.

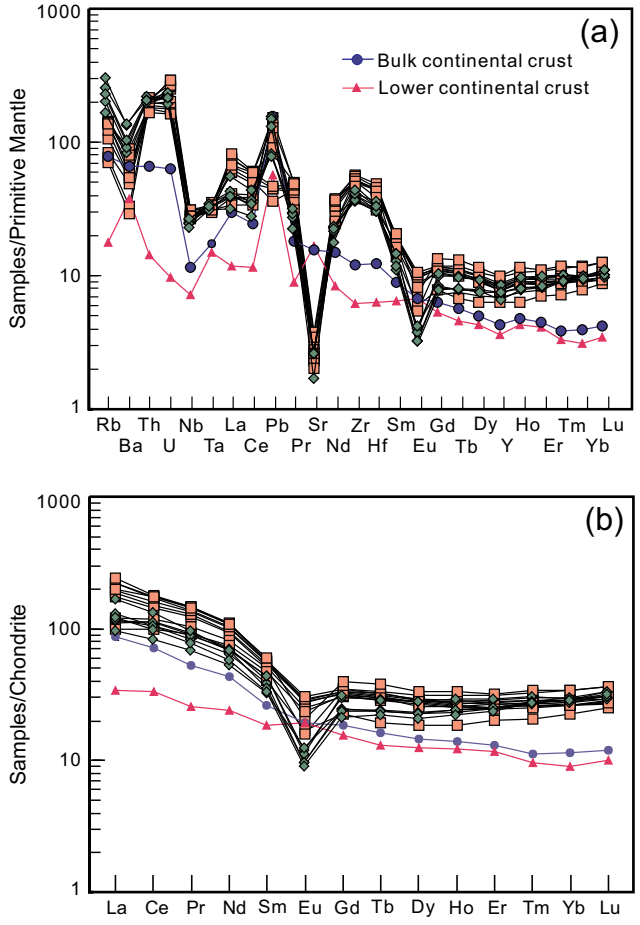

Fig. 5. (a) Spider diagrams of trace elements and (b) REE distribution patterns for the Qunjisayi A-type felsic rocks. Average chondrite and primitive mantle normalizing values are from Sun and McDonough (1989); Compositions of average bulk- and lower continental crust are form Rudnick and Gao (2003) (symbols as in Fig. 4).

5.2.2. Qunjisayi granites

The Qunjisayi granites have also relatively low A/CNK values (Fig. 3b) and lack of aluminous minerals, indicating that they were unlikely to have been generated by partial melting of metasedimentary rocks. The granites have also narrow range of SiO_2 contents (69.9–72.11 wt.%) and Eu/Eu* (0.38–0.69) and low Rb/Sr (0.91–1.89) ratios (Table 4), implying that fractional crystallization was not the major petrogenetic mechanism. Their high $FeO^T/(FeO^T + MgO)$ (Fig. 7a) and moderate K_2O/Na_2O (0.35–0.95) values indicate that they were not derived from a granulite residues or middle to lower crustal rocks sources.

The Qunjisayi granites are characterized by relatively low HREE contents, with $(La/Yb)_N = 3.56–8.41$ (Fig. 5b), suggesting significant amount of residual garnet and/or amphibole in their source region (e.g., Rapp and Watson, 1995; Zhang et al., 2012a). If garnet is the dominated residual mineral in the source, they will have a progressive decrease in HREEs with increasing atomic number (Wu et al., 2006). In contrast, if amphibole is the dominated residual phase in the source, they will show concave-upward patterns between the middle and heavy REEs (Rollinson, 1993). In addition, Amphibole has much higher K_2O contents than garnet in residual phases during high-pressure melting of metabasaltic rocks (Rapp and Watson, 1995), the presence of amphibole in the residue phase can buffer the K_2O concentration in the melt and thus, produce low K_2O/Na_2O ratios granitic melts. The Qunjisayi granites exhibit nearly flat HREEs profiles with $(Tb/Yb)_N = 0.86–1.45$ (Fig. 5b) and have moderate K_2O/Na_2O ratios, suggest that residual amphibole was played an important role in the source. The granites have high positive $\varepsilon_{Nd}(t)$ (+3.8 to +4.3), $\varepsilon_{Hf}(t)$ (+9 to +16) and low $(^{87}Sr/^{86}Sr)_i$ (0.7034–0.7052) values, similar the Carboniferous basalts and *K*-rich rocks from the western Tianshan (Fig. 8a and b), suggesting that they may have been derived from a lower crustal source formed by underplating of depleted mantle-derived basaltic magmas (e.g., Qu et al., 2012; Zhang et al., 2012a; Tang et al., 2014). As a result, we argue that the Qunjisayi granites were generated by partial melting of a juvenile basaltic crustal source in amphibolite stability field. In order to model partial melting of a basaltic crust, we selected the Carboniferous basaltic trachyandesite sample (YX2-6; Yang et al., 2012) form Yuximolegai in the Awulale Mountian ($\varepsilon_{Nd}(t) = 5.4$) as the source of the Qunjisayi granites. As mentioned above, the partial melting took place in stability field of amphibolite. We assumed that the mineral assemblage was Amphibole:Plagioclase:Clinopyroxene = 70:20:10. The chondrite-normalized REE pattern of the average Qunjisayi granites can be reproduced by 10–15% batch melting of the Yuximolegai basaltic trachyandesite, except for having a slightly higher Eu concentrate than the average Qunjisayi granites (Fig. 8c), which may have been caused by the fractionation of plagioclases. In addition, the Qunjisayi granites have positive $\varepsilon_{Hf}(t)$ values with large variation and their highest zircon $(^{176}Hf/^{177}Hf)_i$ ratios (0.283031–0.283037) with U–Pb ages of 292–303 Ma, corresponding to the maximum $\varepsilon_{Hf}(t)$ values of 15.6–16 (Fig. 8b, Table 3), suggesting the involvement of mantle-derived components.

In summary, the Qunjisayi rhyolites may have been formed by partial melting of calc-alkaline granitic crustal rocks juvenile crus-

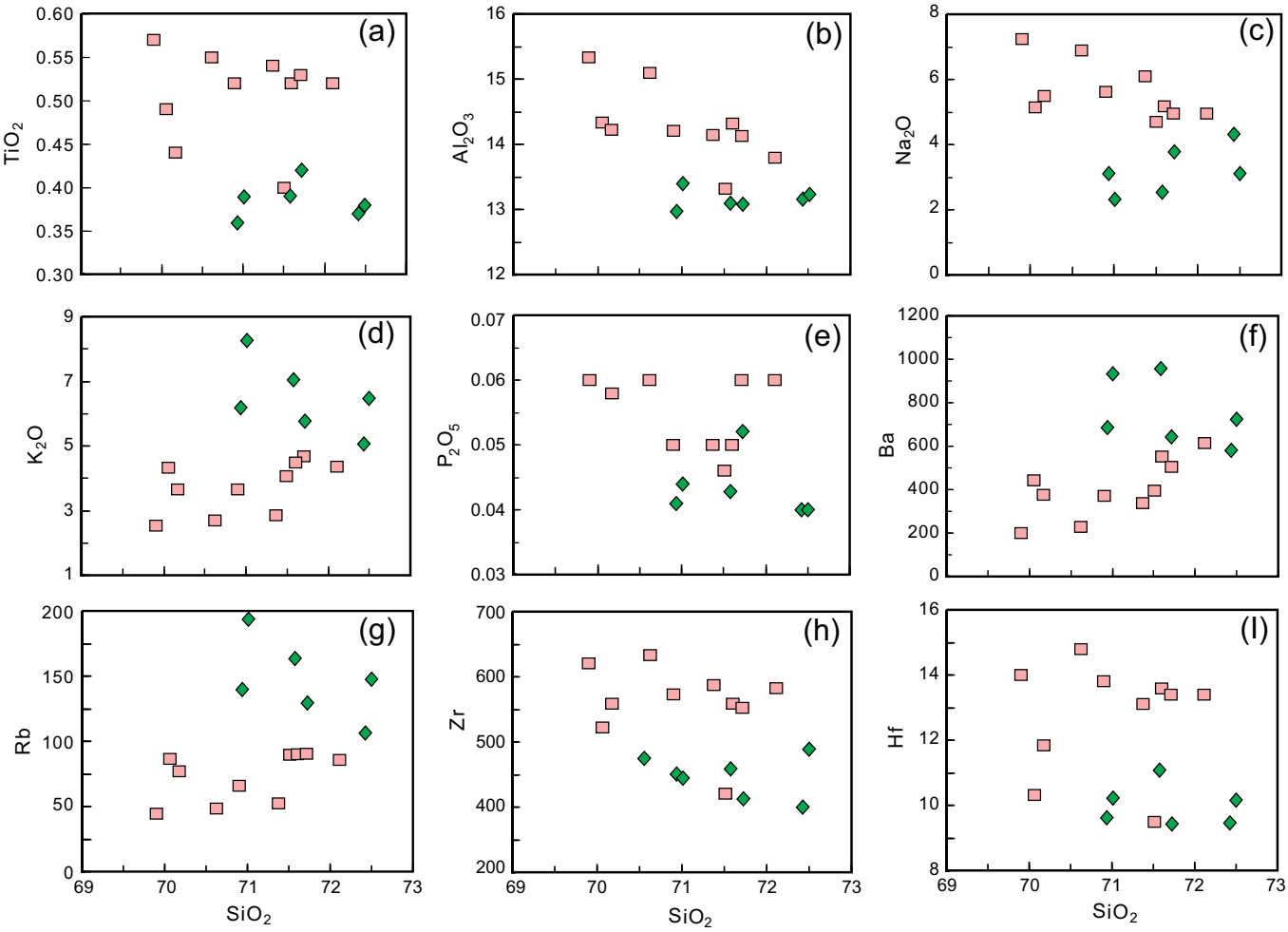

Fig. 6. Harker diagrams of the Qunjisayi A-type felsic rocks (symbols as in Fig. 4).

tal source at low pressure, whereas the Qunjisayi granites are most likely generated by partial melting of basaltic lower crust with some mantle-derived components.

5.3. Tectonic settings

Generation of typical A-type magmatism is commonly related to extensional settings, such as those related to post-collision, intraplate extension, mantle plume and subduction-related extension (Dall'Agnol et al., 2012 and references therein). Eby (1992) has subdivided typical A-type granitoids into the A_1 and A_2 on the basis of their different geochemical characteristics (e.g., Y/Nb ratios). The A_1-type granitoids are generally formed in continental rifts or intraplate settings, whereas the A_2-type granitoids can be formed in variety of tectonic settings, such as in post-collisional stage of an orogeny and even subduction-related settings (Eby, 1992; Zhao et al., 2008a; Shen et al., 2011; Li et al., 2012a). There are two phases of suspected mantle plume activities have been proposed in the Late Paleozoic western Tianshan, including: (1) the Carboniferous phase, related to the proposed large igneous province (LIP) in Tianshan (Xia et al., 2004); (2) the Early Permian phase in Tarim, which has broadly influenced the magmatism in Tarim block and western Tianshan (Yu et al., 2012; Zhang and Zou, 2013). The existence of a suspected Carboniferous mantle plume in western Tianshan is questionable because no unambivalent LIP occurrence has been reported there (Zhu et al., 2009): The Dahalajunshan formation, which has been considered as an important part of the suspected LIP (Xia et al., 2004), has a great variety of volcanic rocks, including basalt, andesite, dacite and rhyolite, with ages spanning across 50 Ma (>361–313 Ma), which is a too long time span for typical LIPs (Zhu et al., 2009). In addition, these rocks have significantly arc-magma features (e.g., Zhu et al., 2006a,b, 2009; Long et al., 2011; Yang et al., 2012). Although the Early Permian LIP may exist in Tarim, our new zircon U–Pb ages of ca. 306–296 Ma for the Qunjisayi felsic rocks are significantly older than the reported Early Permian (ca. 275 Ma) mantle Tarim plume (Zhang et al., 2010). In addition, The Qunjisayi rhyolites have high Y/Nb values (1.6–2.2), suggesting that they belong to A_2-subtype, which are significantly distinct from the Permian (262–277 Ma) A_1-subtype granites that genetically related to the Tarim mantle plume (Fig. 9, Zhang and Zou, 2013). Furthermore, the A_2-subtype granitoids were suggested to form in a post-collisional or subduction-related extensional environment (Eby, 1992; Zhao et al., 2008a; Shen et al., 2011; Li et al., 2012a), different from the within plate A_1-subtype granitoids. Therefore, mantle plume activities were unlikely to be responsible for the Qunjisayi A-type magmatism.

The Late Carboniferous Qunjisayi rhyolites are also unlikely to have formed in a post-collisional setting. The Qunjisayi rhyolites all plot in the volcanic arc field on the the Rb/30–Hf–Ta*3 tectonic discrimination diagram (Fig. 9c). In addition, the approximately coeval rocks in the Awulale Mountain were formed in subduction-related settings, such as the Zhongyangchang mafic dike–granitoid association (310 Ma, Tang et al., 2014) and Yuximulegai quartz diorite (310 Ma, Yang et al., 2012). There is growing evidence for the subduction of the South Tianshan oceanic crust

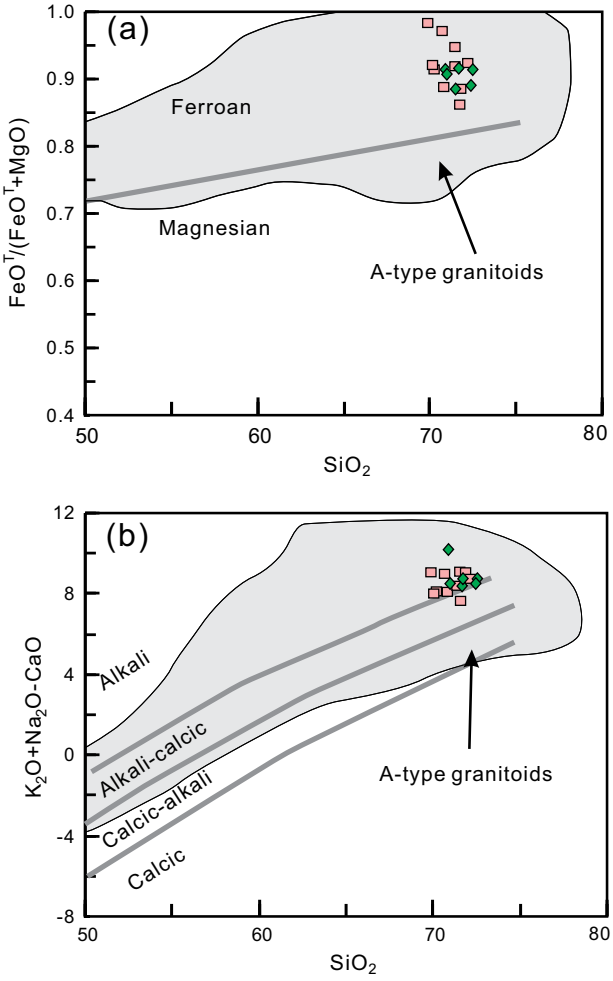

Fig. 7. Geochemical discrimination diagrams for the Qunjisayi A-type felsic rocks, modified after Frost et al. (2001) and Frost and Frost (2011). (Symbols as in Fig. 4).

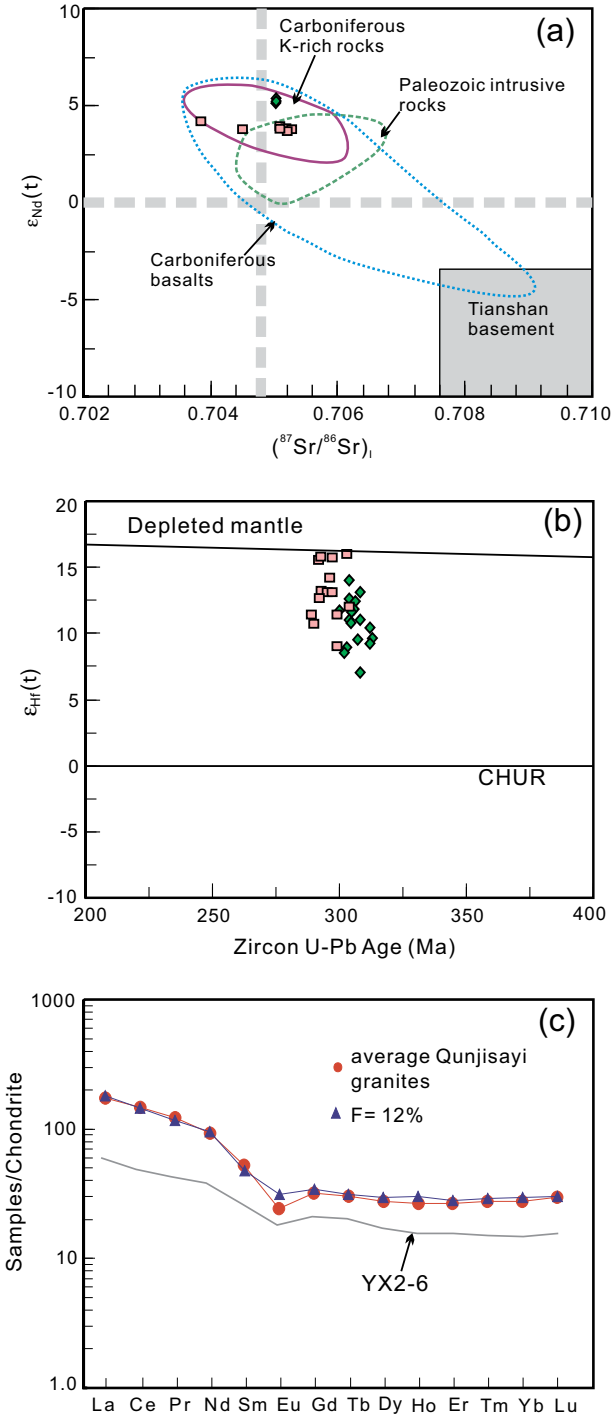

Fig. 8. (a) $\varepsilon_{Nd}(t)$ vs. $(^{87}Sr/^{86}Sr)_i$ diagram for the Qunjisayi A-type felsic rocks (the $(^{87}Sr/^{86}Sr)_i$ values of the Qunjisayi rhyolites are assumed as 0.7051, which is the average values of the Paleozoic intrusive rocks. Data of the Tianshan basement (Hu et al., 2010), Paleozoic intrusive rocks (Zhao et al., 2008b; Tang et al., 2014; Li et al., 2013; Yan et al., 2013), Carboniferous basalts and K-rich rocks (Yang et al., 2012, 2014a and references therein) are also shown for comparison; (b) $\varepsilon_{Hf}(t)$ vs. zircon U–Pb ages diagrams for the Qunjisayi A-type felsic rocks; and (c) model chondrite-normalized REE pattern compared with the Qunjisayi granites. The REE partition coefficients are from McKenzie and O'Nions (1991).

subducted north beneath the western Tianshan lasted until Late Carboniferous (Gao et al., 2009; Xiao et al., 2009, 2010, 2013; Han et al., 2011; Yang et al., 2012). In addition, SHRIMP zircon U–Pb age of 316 ± 3 Ma from the undeformed Sikeshu pluton, which crosscuts the Bayingou ophiolites, well constrains the upper age bound for the time of collision between the YCTB and Junggar block (Han et al., 2010). Therefore, the Carboniferous Qunjisayi rhyolites were more likely to form in an extensional setting affected by the subduction of South Tianshan Ocean, probably a back- or inter-arc basin environment, rather than a post-collisional one.

After the closure of the southern Tianshan Ocean, subsequent magmatism took place in an intraplate environment, perhaps associated with post-collisional extensional events (e.g., Konopelko et al., 2007; Han et al., 2010; Yang et al., 2012). However, the Early Permian Qunjisayi A-type granites also belong to the A_2-subtype (Fig. 9a and b), but are distinct from Early Permian (285 Ma) leucogranite from the South Tianshan Orogen that mainly fall into the POG field (Fig. 9c; Gao et al., 2011) and the Early Permian (289 Ma) A-type granites form the northwestern Tianshan district that all fall into the WPG field (Fig. 9c; Tang et al., 2010). As a result, although the Qunjisayi granites were formed in a post-collisional setting, their formation may have still been effected by the late subduction processes.

Based on our new geochemical and geochronological evidence, we have proposed a Carboniferous–Permian western Tianshan tectonic model for the petrogenesis of the Qunjisayi felsic rocks. As shown in the Fig. 10, the Carboniferous–Permian magmatism in the Tianshan Orogen can be roughly divided into two main episodes encompassing the Late Devonian to Late Carboniferous and the Early Permian, as suggested by a histogram of zircon U–Pb age data. The Late Devonian to Late Carboniferous magmatic episode comprises mainly subduction-related magmatic rocks with

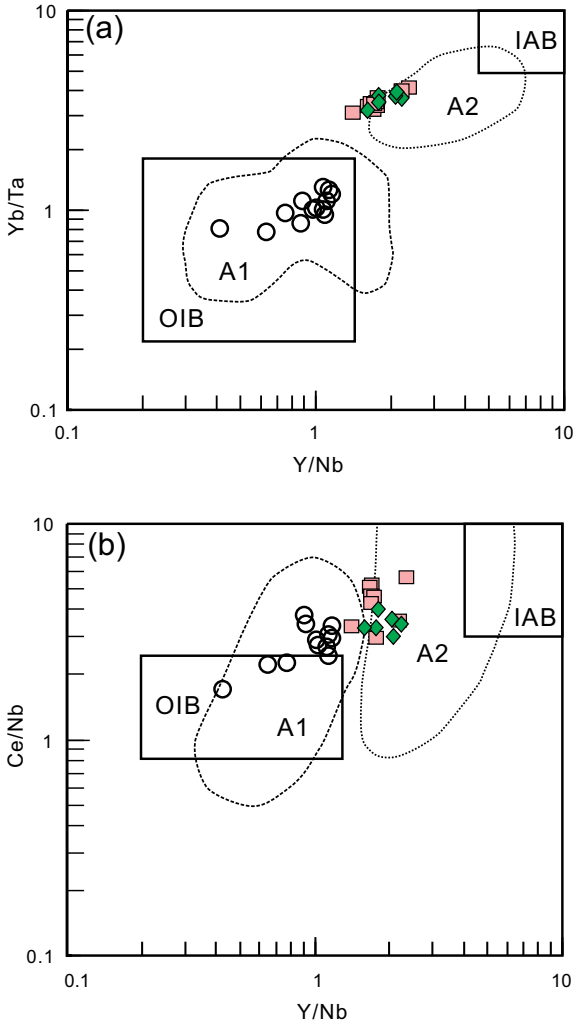

Fig. 9. (a) Yb/Ta vs. Y/Nb and (b) Y/Nb vs. Ce/Nb diagrams for the Qunjisayi A-type felsic rocks (Eby, 1992). The A_1- and A_2-subtype granitoid fields are as defined in of Eby (1990, 1992); (c) Rb/30-Hf-3*Ta diagram of the Qunjisayi A-type felsic rocks. Base map is from Harris et al. (1986). Data for the south Tianshan leucogranite are from Gao et al. (2011) (285 Ma; red circle). Data for the northwestern Tianshan A-type granite are from Tang et al. (2010) (289 Ma; black triangle). Data for the western Tarim A-type granite are from Zhang and Zou (2013) (262–277 Ma; black circles). OIB = oceanic island basalt; IAB = island arc basalt; VAG = volcanic arc granite; WPG = within-plate granite; Syn-COLG = Syn-collision granite; POG = post-orogenic granite (symbols as in Fig. 4). (For interpretation of the references to color in this figure legend, the reader is referred to the web version of this article.)

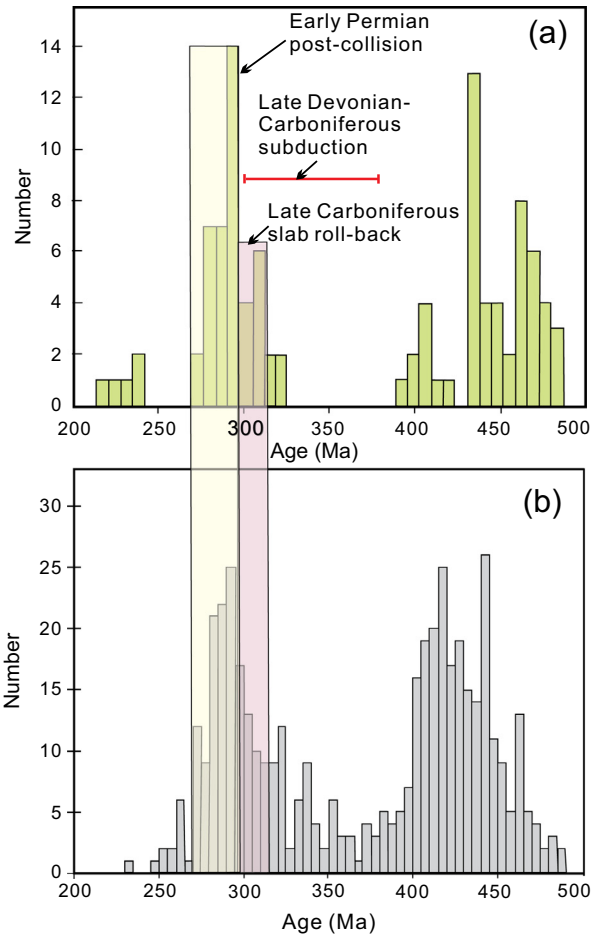

Fig. 10. Schematic histogram of zircon U–Pb age for (a) granitoids (modified after Xiao et al., 2013) and (b) detrital zircons (data sources: Ren et al., 2011 and Wang et al., 2014) of the Tianshan.

typical arc-like geochemical affinities, such as enrichment of large ion lithophile elements (LILEs) and negative anomalies of Ta, Nb and Ti (e.g., Zhu et al., 2009; Niu et al., 2010; Yang et al., 2012; Tang et al., 2014). It is noteworthy that a significant magmatic "flare-up" event occurred during Late Carboniferous in the Tianshan orogen (Fig. 10). In addition, subduction-related mafic rocks, such as the ca. 310 Ma mafic dikes in Zhongyangchang area (Tang et al., 2014), the 313 Ma ferrobasalts and gabbro in the eastern Awulale (Li et al., 2015 and author's unpublished data) and the 306 Ma gabbro in Tekes Country (Zhu et al., 2010), were also formed. These Late Carboniferous mafic rocks were derived from a depleted mantle source with involvements of some asthenospheric components. Generation of A-type rocks, e.g., the Qunjisayi rhyolites, requires a high temperature in their source region, Delamination of thickened lower crust, asthenosphere mantle upwelling and underplating of mafic magma are the most commonly invoked mechanisms to account for raising the local geothermal gradient (Thompson, 1999). Taking into account all available data, we prefer that a slab roll-back during the Late Carboniferous in western Tianshan was likely responsible for the generation of the Qunjisayi rhyolites and coeval magmatic "flare-up" (Fig. 11a). The slab roll-back event may have disturbed the mantle wedge and induced asthenospheric upwelling. The upwelling, in turn, may have induced the underplating of mafic magmas, which provided the necessary heat for crustal partial melting and finally produced the Qunjisayi rhyolites. The later Permian magmatic episode contains voluminous post-collisional granitoids and mafic rocks (Zhao et al., 2003, 2008b; Yang et al., 2012; Li et al., 2013),

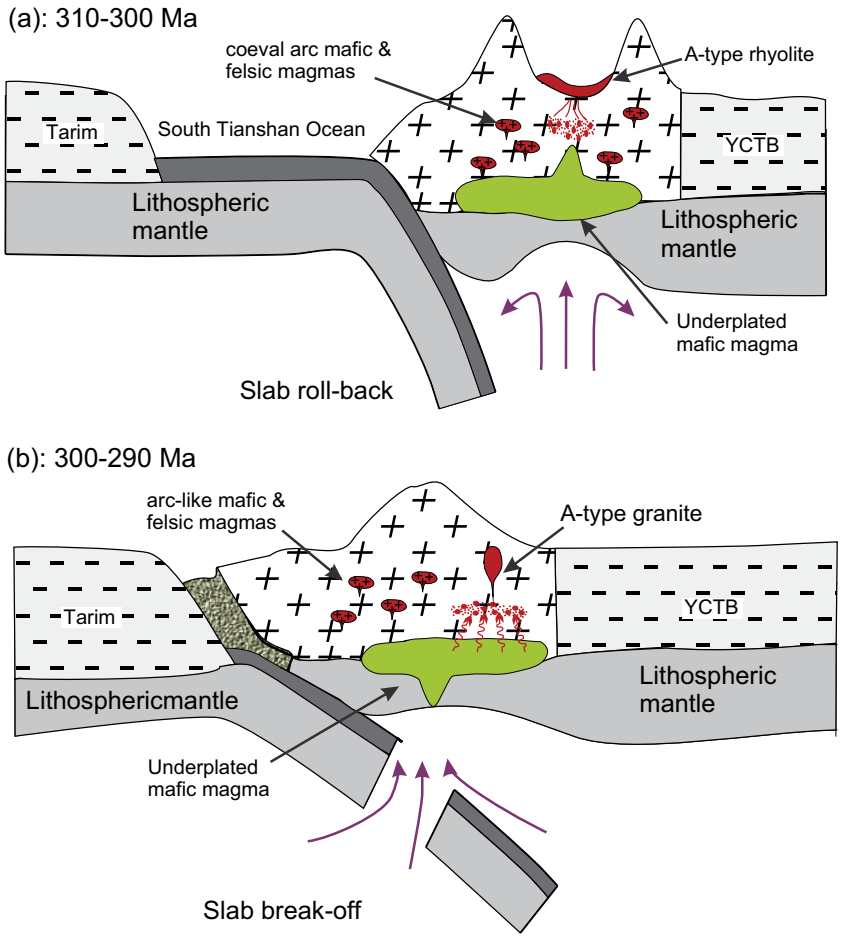

Fig. 11. Schematic diagrams for the Late Paleozoic tectonic evolution of western Tianshan.

and lack of arc-related rocks (Zhao et al., 2008b). During ca. 300–290 Ma, the incipient collision between the YCTB and Tarim blocks may have occurred (Fig. 11b; e.g., Gao et al., 2009; Luo et al., 2010; Yang et al., 2012). Due to the increase of downward traction (Van Hunen and Allen, 2011), the subducted slab may have broken off, and thus may have allowed even further asthenospheric upwelling and magmatism (Figs. 10 and 11b). The asthenospheric upwelling, triggered by slab break-off, may have led to the partial melting of the mantle wedge to form hot and relatively depleted magmas. These depleted magmas provide necessary heat and materials for generating the Qunjisayi granites (Fig. 11b). In addition, a slab break-off model can readily account for the occurrence of Early Permian Na-rich basaltic (Author's unpublished data) and trachy-andesitic rocks (Yang et al., 2012), with deleted Sr–Nd isotopic composition and ocean island basalt (OIB)-like REE patterns in the Awulale Mountain. Therefore, the geodynamic setting of the western Tianshan was transformed to a post-collision lithospheric extensional regime during Early Permian.

6. Conclusions

1. Two episodes of A_2-type magmatism are identified in Qunjisayi, western Tianshan. The earlier rhyolites were erupted in the Late Carboniferous (ca. 306 Ma) and the later granites were emplaced in the Early Permian (ca. 296 Ma). Both suites belong to the A_2-subtype granitoids.
2. The Qunjisayi rhyolites may have been generated by partial melting of a juvenile calc-alkaline granitic crustal rocks in a plagioclase stability field, triggered by subduction slab roll-back.
3. The Qunjisayi granites may have a lower crustal source with some depleted mantle-derived components. Asthenospheric upwelling, induced by slab break-off, may have played a critical role for the formation of the granites.

Acknowledgments

We sincerely thank two anonymous for their constructive and helpful reviews on this manuscript. We also thank G.Q. Hu, H. Zhang, X.L. Tu, and J.L. Ma for helping with the analytical works. This work was financially supported by the National Natural Science Foundation of China (Grants U1203291, 41373031 and 41173040). This is the contribution No. IS-2014 from GIGCAS.

References

Agnol, R.D., de Oliveira, D.C., 2007. Oxidized, magnetite-series, rapakivi-type granites of Carajas, Brazil: implications for classification and petrogenesis of A-type granites. Lithos 93, 215–233.
An, F., Zhu, Y.F., Wei, S.N., Lai, S.C., 2013. An early Devonian to early carboniferous volcanic arc in North Tianshan, NW China: geochronological and geochemical evidence from volcanic rocks. J. Asian Earth Sci. 78, 100–113.
Barboni, M., Bussy, F., 2013. Petrogenesis of magmatic albite granites associated to cogenetic A-type granites: Na-rich residual melt extraction from a partially crystallized A-type granite mush. Lithos 177, 328–351.
Belousova, E., Griffin, W., O'reilly, S.Y., Fisher, N., 2002. Igneous zircon: trace element composition as an indicator of source rock type. Contrib. Miner. Petrol. 143, 602–622.
Bi, X., Hu, R., Ye, Z., Shao, S., 2000. Relations between A-type granites and copper mineralization as exemplified by the Machangqing Cu deposit. Sci. China, Ser. D Earth Sci. 43, 93–102.

Black, L.P., Kamo, S.L., Allen, C.M., Davis, D.W., Aleinikoff, J.N., Valley, J.W., Mundil, R., Campbell, I.H., Korsch, R.J., Williams, I.S., Foudoulis, C., 2004. Improved $^{206}Pb/^{238}U$ microprobe geochronology by the monitoring of a trace-element-related matrix effect; SHRIMP, ID–TIMS, ELA–ICP–MS and oxygen isotope documentation for a series of zircon standards. Chem. Geol. 205, 115–140.

Bonin, B., 2007. A-type granites and related rocks: evolution of a concept, problems and prospects. Lithos 97, 1–29.

Cawood, P.A., Kröner, A., Collins, W.J., Kusky, T.M., Mooney, W.D., Windley, B.F., 2009. Accretionary orogens through earth history. Geol. Soc., London, Spec. Publ. 318, 1–36.

Chappell, B.W., White, A.J.R., Wyborn, D., 1987. The importance of residual source material (restite) in granite petrogenesis. J. Petrol. 28, 1111–1138.

Clemens, J., Holloway, J.R., White, A., 1986. Origin of an A-type granite; experimental constraints. Am. Mineral. 71, 317.

Collins, W., Beams, S., White, A.J.R., Chappell, B., 1982. Nature and origin of A-type granites with particular reference to southeastern Australia. Contrib. Miner. Petrol. 80, 189–200.

Creaser, R.A., Price, R.C., Wormald, R.J., 1991. A-type granites revisited: assessment of a residual-source model. Geology 19, 163–166.

Dall'Agnol, R., Teixeira, N.P., Ramo, O.T., Moura, C.A.V., Macambira, M.J.B., de Oliveira, D.C., 2005. Petrogenesis of the Paleoproterozoic rapakivi A-type granites of the Archean Carajas metallogenic province, Brazil. Lithos 80, 101–129.

Dall'Agnol, R., Frost, C.D., Ramo, O.T., 2012. IGCP Project 510 "A-type granites and related rocks through time": Project vita, results, and contribution to granite research. Lithos 151, 1–16.

Eby, G.N., 1990. The A-type granitoids – a review of their occurrence and chemical characteristics and speculations on their petrogenesis. Lithos 26, 115–134.

Eby, G.N., 1992. Chemical subdivision of the A-type granitoids: petrogenetic and tectonic implications. Geology 20, 641.

Espinoza, F., Morata, D., Polve, M., Lagabrielle, Y., Maury, R.C., Guivel, C., Cotten, J., Bellon, H., Suarez, M., 2008. Bimodal back-arc alkaline magmatism after ridge subduction: Pliocene felsic rocks from Central Patagonia (47 degrees S). Lithos 101, 191–217.

Frost, C.D., Frost, B.R., 1997. Reduced rapakivi-type granites: the tholeiite connection. Geology 25, 647–650.

Frost, C.D., Frost, B.R., 2011. On ferroan (A-type) granitoids: their compositional variability and modes of origin. J. Petrol. 52, 39.

Frost, B.R., Barnes, C.G., Collins, W.J., Arculus, R.J., Ellis, D.J., Frost, C.D., 2001. A geochemical classification for granitic rocks. J. Petrol. 42, 2033–2048.

Gao, J., Li, M.S., Xiao, X.C., Tang, Y.Q., He, G.Q., 1998. Paleozoic tectonic evolution of the Tianshan Orogen, northwestern China. Tectonophysics 287, 213–231.

Gao, J., Long, L.L., Klemd, R., Qian, Q., Liu, D.Y., Xiong, X.M., Su, W., Liu, W., Wang, Y.T., Yang, F.Q., 2009. Tectonic evolution of the South Tianshan orogen and adjacent regions, NW China: geochemical and age constraints of granitoid rocks. Int. J. Earth Sci., 1221–1238

Gao, J., Klemd, R., Qian, Q., Zhang, X., Li, J., Jiang, T., Yang, Y., 2011. The collision between the Yili and Tarim blocks of the Southwestern Altaids: geochemical and age constraints of a leucogranite dike crosscutting the HP–LT metamorphic belt in the Chinese Tianshan Orogen. Tectonophysics 499, 118–131.

Han, B.F., Guo, Z.J., Zhang, Z.C., Zhang, L., Chen, J.F., Song, B., 2010. Age, geochemistry, and tectonic implications of a Late Paleozoic stitching pluton in the North Tian Shan suture zone, western China. Geol. Soc. Am. Bull. 122, 627–640.

Han, B.F., He, G.Q., Wang, X.C., Guo, Z.J., 2011. Late Carboniferous collision between the Tarim and Kazakhstan–Yili terranes in the western segment of the South Tian Shan Orogen, Central Asia, and implications for the Northern Xinjiang, western China. Earth Sci. Rev. 109, 74–93.

Harris, N.B., Pearce, J.A., Tindle, A.G., 1986. Geochemical characteristics of collision-zone magmatism. Geol. Soc., London, Spec. Publ. 19, 67–81.

Hendrix, M.S., Dumitru, T.A., Graham, S.A., 1994. Late Oligocene-early Miocene unroofing in the Chinese Tian Shan: an early effect of the India–Asia collision. Geology 22, 487–490.

Hu, A., Wei, G., Jahn, B., Zhang, J., Deng, W., Chen, L., 2010. Formation of the 0.9 Ga Neoproterozoic granitoids in the Tianshan Orogen, NW China: constraints from the SHRIMP zircon age determination and its tectonic significance. Geochimica 39, 197–211 (in Chinese with English abstract).

Huang, H.Q., Li, X.H., Li, W.X., Li, Z.X., 2011. Formation of high ^{18}O fayalite-bearing A-type granite by high-temperature melting of granulitic metasedimentary rocks, southern China. Geology 39, 903.

Jahn, B.M., 2004. The Central Asian Orogenic Belt and growth of the continental crust in the Phanerozoic. Geol. Soc., London, Spec. Publ. 226, 73–100.

Jahn, B.M., Wu, F., Chen, B., 2000. Massive granitoid generation in Central Asia: Nd isotope evidence and implication for continental growth in the Phanerozoic. Episodes 23, 82–92.

Jiang, N., Zhang, S.Q., Zhou, W.G., Liu, Y.S., 2009. Origin of a Mesozoic granite with A-type characteristics from the North China craton: highly fractionated from I-type magmas? Contrib. Miner. Petrol. 158, 113–130.

Jiang, T., Gao, J., Klemd, R., Qian, Q., Zhang, X., Xiong, X., Wang, X., Tan, Z., Chen, B., 2014. Paleozoic ophiolitic mélanges from the South Tianshan Orogen, NW China: geological, geochemical and geochronological implications for the geodynamic setting. Tectonophysics 612–613, 106–127.

Jung, S., Mezger, K., Hoernes, S., 1998. Petrology and geochemistry of syn- to post-collisional metaluminous A-type granites—a major and trace element and Nd–Sr–Pb–O-isotope study from the Proterozoic Damara Belt, Namibia. Lithos 45, 147–175.

King, P.L., White, A.J.R., Chappell, B.W., Allen, C.M., 1997. Characterization and origin of aluminous A-type granites from the Lachlan Fold Belt, Southeastern Australia. J. Petrol. 38, 371–391.

King, P., Chappell, B., Allen, C., White, A., 2001. Are A-type granites the high-temperature felsic granites? Evidence from fractionated granites of the Wangrah Suite. Aust. J. Earth Sci. 48, 501–514.

Konopelko, D., Biske, G., Seltmann, R., Eklund, O., Belyatsky, B., 2007. Hercynian post-collisional A-type granites of the Kokshaal Range, Southern Tien Shan, Kyrgyzstan. Lithos 97, 140–160.

Kroner, A., Kovach, V., Belousova, E., Hegner, E., Armstrong, R., Dolgopolova, A., Seltmann, R., Alexeiev, D.V., Hoffmann, J.E., Wong, J., Sun, M., Cai, K., Wang, T., Tong, Y., Wilde, S.A., Degtyarev, K.E., Rytsk, E., 2014. Reassessment of continental growth during the accretionary history of the Central Asian Orogenic Belt. Gondwana Res. 25, 103–125.

Lei, R.X., Wu, C.Z., Gu, L.X., Zhang, Z.Z., Chi, G.X., Jiang, Y.H., 2011. Zircon U–Pb chronology and Hf isotope of the Xingxingxia granodiorite from the Central Tianshan zone (NW China): Implications for the tectonic evolution of the southern Altaids. Gondwana Res. 20, 582–593.

Li, X.H., 1997. Geochemistry of the Longsheng Ophiolite from the southern margin of Yangtze Craton, SE China. Geochem. J. Jpn. 31, 323–338.

Li, X., Qi, C., Liu, Y., Liang, X., Tu, X., Xie, L., Yang, Y., 2005. Petrogenesis of the Neoproterozoic bimodal volcanic rocks along the western margin of the Yangtze Block: new constraints from Hf isotopes and Fe/Mn ratios. Chin. Sci. Bull. 50, 2481–2486.

Li, H., Ling, M., Li, C., Zhang, H., Ding, X., Yang, X., Fan, W., Li, Y., Sun, W., 2012a. A-type granite belts of two chemical subgroups in central eastern China: indication of ridge subduction. Lithos 150, 26–36.

Li, X.Y., Xu, X.Y., Sun, J.M., Li, Z.P., Bai, J.K., Zhang, X.B., 2012b. Geochemistry and dating of the hypabyssal granite body in Nilka County of Western Tianshan Mountains. Geol. Bull. China, 1939–1948 (in Chinese with English abstract).

Li, N.B., Niu, H.C., Shan, Q., Jiang, Y.H., Zeng, L.J., Yang, W.B., J, F.Z., 2013. Zircon U–Pb geochronology and geochemistry of post-collisional granitic porphyry from Yuantoushan, Nileke, Xinjiang province. Acta Petrol. Sin. 29, 3402–3412 (in Chinese with English abstract).

Li, N.B., Niu, H.C., Zhang, X.C., Zeng, Q.S., Shan, Q., Li, C.Y., Yan, S., Yang, W.B., 2015. Age, petrogenesis and tectonic significance of the ferrobasalts in the Chagangnuoer iron deposit, western Tianshan. Int. Geol. Rev. http://dx.doi.org/10.1080/00206814.2015.1004136 (In press).

Liang, X.R., Wei, G.J., Li, X.H., Liu, Y., 2003. Precise measurement of $^{143}Nd/^{144}Nd$ and Sm/Nd ratios using multiple-collectors inductively coupled plasma-mass spectrometer (MC–ICPMS). Geochimica 32, 91–96 (in Chinese with English abstract).

Liu, S.W., Guo, Z.J., Zhang, Z.C., Li, Q.G., Zheng, H.F., 2004. Nature of the Precambrian metamorphic blocks in the eastern segment of Central Tianshan: constraint from geochronology and Nd isotopic geochemistry. Sci. China, Ser. D Earth Sci. 47, 1085–1094.

Liu, Y.S., Hu, Z.C., Gao, S., Gunther, D., Xu, J., Gao, C.G., Chen, H.H., 2008. In situ analysis of major and trace elements of anhydrous minerals by LA-ICP-MS without applying an internal standard. Chem. Geol. 257, 34–43.

Liu, Y., Gao, S., Hu, Z., Gao, C., Zong, K., Wang, D., 2010. Continental and oceanic crust recycling-induced melt–peridotite interactions in the Trans-North China Orogen: U–Pb dating, Hf isotopes and trace elements in zircons from mantle xenoliths. J. Petrol. 51, 537–571.

Liu, X., Qian, Q., Su, W., Li, J.L., 2012. Pluton from Muhanbasitao in the western of Awulale, Western Tianshan: geochemistry, geochronology and geological implications. Acta Petrol. Sin. 28, 2401–2413 (in Chinese with English abstract).

Loiselle, M., Wones, D., 1979. Characteristics and origin of anorogenic granites. Geol. Soc. Am. Abstr. Programs 11, 468.

Long, L., Gao, J., Klemd, R., Beier, C., Qian, Q., Zhang, X., Wang, J., Jiang, T., 2011. Geochemical and geochronological studies of granitoid rocks from the Western Tianshan Orogen: implications for continental growth in the southwestern Central Asian Orogenic Belt. Lithos 126, 321–340.

Lu, S.N., Li, H.K., Zhang, C.L., Niu, G.H., 2008. Geological and geochronological evidence for the Precambrian evolution of the Tarim Craton and surrounding continental fragments. Precambr. Res. 160, 94–107.

Lu, H.H., Chang, Y.A., Wang, W., Zhou, Z.Y., 2013. Rapid exhumation of the Tianshan Mountains since the early Miocene: evidence from combined apatite fission track and (U–Th)/He thermochronology. Sci. China-Earth Sci. 56, 2116–2125.

Ludwig, K., 2008. Isoplot 3.6; A Geochronology Toolkit for Microsoft Excel. Berkeley Geochronology Center, p. 77.

Luo, Y., Niu, H.C., Yang, W.B., Zhang, B., Zhou, C.P., Liao, S.P., Yu, X.Y., 2010. Geochemical characteristics and petrogenesis of the Aikendaban Permian shoshonite in the western Tianshan. Acta Petrol. Sin. 26, 2925–2934 (in Chinese with English abstract).

Ma, X., Shu, L., Santosh, M., Li, J., 2012. Detrital zircon U–Pb geochronology and Hf isotope data from Central Tianshan suggesting a link with the Tarim Block: implications on Proterozoic supercontinent history. Precambr. Res. 206–207, 1–16.

Mckenzie, D., O'Nions, R.K., 1991. Partial melt distributions from inversion of rare-earth element concentrations. J. Petrol. 32, 1021–1091.

Moghazi, A., Harbi, H., Ali, K., 2011. Geochemistry of the Late Neoproterozoic Hadb adh Dayheen ring complex, Central Arabian Shield: implications for the origin of rare-metal-bearing post-orogenic A-type granites. J. Asian Earth Sci. 42, 1324–1340.

Niu, H.C., Shan, Q., Luo, Y., Yang, W.B., Zhou, C.P., Liao, S.P., Yu, X.Y., 2010. Geochronological and geochemical studies on quartz diorite in Yuximolegai

Daban, West Tianshan and its tectonic implication. Acta Petrol. Sin. 26, 2935–2945 (in Chinese with English abstract).
Patiño Douce, A.E., 1997. Generation of metaluminous A-type granites by low-pressure melting of calc-alkaline granitoids. Geology 25, 743–746.
Patiño Douce, A.E., 1999. What do experiments tell us about the relative contributions of crust and mantle to the origin of granitic magmas? Geol. Soc., London, Spec. Publ. 168, 55–75.
Peccerillo, A., Barberio, M.R., Yirgu, G., Ayalew, D., Barbieri, M., Wu, T.W., 2003. Relationships between mafic and peralkaline silicic magmatism in continental rift settings: a petrological, geochemical and isotopic study of the Gedemsa volcano, central Ethiopian rift. J. Petrol. 44, 2003–2032.
Pirajno, F., Mao, J., Zhang, Z., Zhang, Z., Chai, F., 2008. The association of mafic–ultramafic intrusions and A-type magmatism in the Tian Shan and Altay orogens, NW China: implications for geodynamic evolution and potential for the discovery of new ore deposits. J. Asian Earth Sci. 32, 165–183.
Qian, Q., Gao, J., Klemd, R., He, G., Song, B., Liu, D., Xu, R., 2009. Early Paleozoic tectonic evolution of the Chinese South Tianshan Orogen: constraints from SHRIMP zircon U–Pb geochronology and geochemistry of basaltic and dioritic rocks from Xiate, NW China. Int. J. Earth Sci. 98, 551–569.
Qu, X.M., Wang, R.J., Xin, H.B., Jiang, J.H., Chen, H., 2012. Age and petrogenesis of A-type granites in the middle segment of the Bangonghu–Nujiang suture, Tibetan plateau. Lithos 146, 264–275.
Rapp, R.P., Watson, E.B., 1995. Dehydration melting of metabasalt at 8–32 kbar – implications for continental growth and crust–mantle recycling. J. Petrol. 36, 891–931.
Ren, R., Han, B.F., Ji, J.Q., Zhang, L., Xu, Z., Su, L., 2011. U–Pb age of detrital zircons from the Tekes River, Xinjiang, China, and implications for tectonomagmatic evolution of the South Tian Shan Orogen. Gondwana Res. 19, 460–470.
Rollinson, H.R., 1993. Using Geochemical Data: Evaluation, Presentation, Interpretation. Longman Singapore Publishers (Pte) Ltd., Singapore, pp. 1–352.
Rudnick, R., Gao, S., 2003. Composition of the continental crust. Treatise Geochem. 3, 1–64.
Sengor, A.M.C., Natalin, B.A., Burtman, V.S., 1993. Evolution of the Altaid Tectonic Collage and Paleozoic Crustal Growth in Eurasia. Nature 364, 299–307.
Shen, X., Zhang, H., Wang, Q., Wyman, D.A., Yang, Y., 2011. Late Devonian–Early Permian A-type granites in the southern Altay Range, Northwest China: petrogenesis and implications for tectonic setting of "A2 sub-type" granites. J. Asian Earth Sci. 42, 986–1007.
Skjerlie, K.P., Johnston, A.D., 1993. Fluid-absent melting behavior of an F-rich tonalitic gneiss at mid-crustal pressures: implications for the generation of anorogenic granites. J. Petrol. 34, 785–815.
Sobel, E.R., Chen, J., Heermance, R.V., 2006. Late Oligocene–early Miocene initiation of shortening in the Southwestern Chinese Tian Shan: implications for Neogene shortening rate variations. Earth Planet. Sci. Lett. 247, 70–81.
Sun, S.S., McDonough, W., 1989. Chemical and isotopic systematics of oceanic basalts: implications for mantle composition and processes. Geol. Soc., London, Spec. Publ. 42, 313–345.
Sun, Y., Ma, C.Q., Liu, Y.Y., She, Z.B., 2011. Geochronological and geochemical constraints on the petrogenesis of late Triassic aluminous A-type granites in southeast China. J. Asian Earth Sci. 42, 1117–1131.
Tang, G.J., Wang, Q., Wyman, D.A., Sun, M., Li, Z.X., Zhao, Z.H., Sun, W.D., Jia, X.H., Jiang, Z.Q., 2010. Geochronology and geochemistry of Late Paleozoic magmatic rocks in the Lamasu–Dabate area, northwestern Tianshan (west China): evidence for a tectonic transition from arc to post-collisional setting. Lithos 119, 393–411.
Tang, G.J., Chung, S.L., Wang, Q., Wyman, D.A., Dan, W., Chen, H.Y., Zhao, Z.H., 2014. Petrogenesis of a Late Carboniferous mafic dike–granitoid association in the western Tianshan: response to the geodynamics of oceanic subduction. Lithos 202–203, 85–99.
Taylor, S.R., McLennan, S.M., 1985. The Continental Crust: Its Composition and Evolution. Blackwell Scientific Publications, Oxford, 312 pp.
Thompson, A.B., 1999. Some time-space relationships for crustal melting and granitic intrusion at various depths. Geol. Soc., London, Spec. Publ. 168, 7–25.
Tu, X., Zhang, H., Deng, W., Ling, M., Liang, H., Liu, Y., Sun, W., 2011. Application of RESOlution in-situ laser ablation ICP-MS in trace element analyses. Geochimica 40, 83–98 (in Chinese with English abstract).
Turner, S., Foden, J., Morrison, R., 1992. Derivation of some A-type magmas by fractionation of basaltic magma: an example from the Padthaway Ridge, South Australia. Lithos 28, 151–179.
Van Hunen, J., Allen, M.B., 2011. Continental collision and slab break-off: a comparison of 3-D numerical models with observations. Earth Planet. Sci. Lett. 302, 27–37.
Wang, Q., Wyman, D.A., Li, Z.X., Bao, Z.W., Zhao, Z.H., Wang, Y.X., Jian, P., Yang, Y.H., Chen, L.L., 2010. Petrology, geochronology and geochemistry of ca. 780 Ma A-type granites in South China: petrogenesis and implications for crustal growth during the breakup of the supercontinent Rodinia. Precambr. Res. 178, 185–208.
Wang, M., Zhang, J., Liu, K., 2014. Continuous denudation and pediplanation of the Chinese Western Tianshan orogen during Triassic to Middle Jurassic: integrated evidence from detrital zircon age and heavy mineral chemical data. J. Asian Earth Sci. http://dx.doi.org/10.1016/j.jseaes.2014.05.013 (in press).
Watson, E.B., 1979. Zircon saturation in felsic liquids: experimental results and applications to trace element geochemistry. Contrib. Miner. Petrol. 70, 407–419.
Watson, E.B., Harrison, T.M., 1983. Zircon saturation revisited: temperature and composition effects in a variety of crustal magma types. Earth Planet. Sci. Lett. 64, 295–304.
Wei, G.J., Liang, X.R., Li, X.H., Liu, Y., 2002. Precise measurement of Sr isotopic composition of liquid and solid base using (LA) MC-ICPMS. Geochimica 31, 295–305 (in Chinese with English abstract).
Whalen, J.B., Currie, K.L., Chappell, B.W., 1987. A-type granites: geochemical characteristics, discrimination and petrogenesis. Contrib. Miner. Petrol. 95, 407–419.
Wiedenbeck, M., AllÉ, P., Corfu, F., Griffin, W.L., Meier, M., Oberli, F., Quadt, A.V., Roddick, J.C., Spiegel, W., 1995. Three natural zircon standards for U–Tu–Pb, Lu–Hf, trace element and REE analyses. Geostand. Newsletter 19, 1–23.
Wilhem, C., Windley, B.F., Stampfli, G.M., 2012. The Altaids of Central Asia: a tectonic and evolutionary innovative review. Earth Sci. Rev. 113, 303–341.
Windley, B.F., Alexeiev, D., Xiao, W.J., Kroner, A., Badarch, G., 2007. Tectonic models for accretion of the Central Asian Orogenic Belt. J. Geol. Soc. 164, 31–47.
Wnrrn, A., 1986. Origin of an A-type granite: experimental constraints. Am. Mineral. 71, 317–324.
Wu, F.Y., Sun, D.Y., Li, H.M., Jahn, B.M., Wilde, S., 2002. A-type granites in northeastern China: age and geochemical constraints on their petrogenesis. Chem. Geol. 187, 143–173.
Wu, R.X., Zheng, Y.F., Wu, Y.B., Zhao, Z.F., Zhang, S.B., Liu, X.M., Wu, F.Y., 2006. Reworking of juvenile crust: element and isotope evidence from Neoproterozoic granodiorite in South China. Precambr. Res. 146, 179–212.
Xia, L.Q., Xu, X.Y., Xia, Z.C., Li, X.M., Ma, Z.P., Wang, L.S., 2004. Petrogenesis of Carboniferous rift-related volcanic rocks in the Tianshan, northwestern China. Geol. Soc. Am. Bull. 116, 419–433.
Xiao, W.J., Windley, B.F., Huang, B.C., Han, C.M., Yuan, C., Chen, H.L., Sun, M., Sun, S., Li, J.L., 2009. End-Permian to mid-Triassic termination of the accretionary processes of the southern Altaids: implications for the geodynamic evolution, Phanerozoic continental growth, and metallogeny of Central Asia. Int. J. Earth Sci. 98, 1189–1217.
Xiao, W.J., Huang, B.C., Han, C.M., Sun, S., Li, J.L., 2010. A review of the western part of the Altaids: a key to understanding the architecture of accretionary orogens. Gondwana Res. 18, 253–273.
Xiao, W.J., Windley, B.F., Allen, M.B., Han, C.M., 2013. Paleozoic multiple accretionary and collisional tectonics of the Chinese Tianshan orogenic collage. Gondwana Res. 23, 1316–1341.
Yan, Y.H., Xue, C.J., Zhang, Z.C., Ding, Z.X., Yang, W.H., Han, Z.H., 2013. Geochemistry and genesis of the Qunjisayi granite porphyry in the west of Awulale area, Western Tianshan Mountains. Acta Petrol. Miner. 32, 139–153 (in Chinese with English abstract).
Yang, W.B., Niu, H.C., Shan, Q., Luo, Y., Sun, W.D., Li, C.Y., Li, N.B., Yu, X.Y., 2012. Late Paleozoic calc-alkaline to shoshonitic magmatism and its geodynamic implications, Yuximolegai area, western Tianshan, Xinjiang. Gondwana Res. 22, 325–340.
Yang, W.B., Niu, H.C., Shan, Q., Chen, H.Y., Hollings, P., Li, N.B., Yan, S., Zartman, R.E., 2014a. Geochemistry of primary-carbonate bearing K-rich igneous rocks in the Awulale Mountains, western Tianshan: Implications for carbon-recycling in subduction zone. Geochim. Cosmochim. Acta 143, 143–164.
Yang, W.B., Niu, H.C., Shan, Q., Sun, W.D., Zhang, H., Li, N.B., Jiang, Y.H., Yu, X.A., 2014b. Geochemistry of magmatic and hydrothermal zircon from the highly evolved Baerzhe alkaline granite: implications for Zr–REE–Nb mineralization. Miner. Deposita 49, 451–470.
Yu, J., Mo, X., Yu, X., Dong, G., Fu, Q., Xing, F., 2012. Geochemical characteristics and petrogenesis of Permian basaltic rocks in Keping area, Western Tarim basin: a record of plume–lithosphere interaction. J. Earth Sci. 23, 442–454.
Yuan, H., Gao, S., Liu, X., Li, H., Günther, D., Wu, F., 2004. Accurate U–Pb age and trace element determinations of zircon by laser ablation-inductively coupled plasma-mass spectrometry. Geostand. Geoanal. Res. 28, 353–370.
Yuan, H.L., Gao, S., Dai, M.N., Zong, C.L., Günther, D., Fontaine, G.H., Liu, X.M., Diwu, C., 2008. Simultaneous determinations of U–Pb age, Hf isotopes and trace element compositions of zircon by excimer laser-ablation quadrupole and multiple-collector ICP-MS. Chem. Geol. 247, 100–118.
Zhang, C.L., Zou, H.B., 2013. Permian A-type granites in Tarim and western part of Central Asian Orogenic Belt (CAOB): genetically related to a common Permian mantle plume? Lithos 172–173, 47–60.
Zhang, C.L., Xu, Y.G., Li, Z.X., Wang, H.Y., Ye, H.M., 2010. Diverse Permian magmatism in the Tarim Block, NW China: Genetically linked to the Permian Tarim mantle plume? Lithos 119, 537–552.
Zhang, D.Y., Zhang, Z.C., Encarnacion, J., Xue, C.J., Duan, S.G., Zhao, Z.D., Liu, J.L., 2012a. Petrogenesis of the Kekesai composite intrusion, western Tianshan, NW China: implications for tectonic evolution during Late Paleozoic time. Lithos 146, 65–79.
Zhang, X., Tian, J., Gao, J., Klemd, R., Dong, L., Fan, J., Jiang, T., Hu, C., Qian, Q., 2012b. Geochronology and geochemistry of granitoid rocks from the Zhibo syngenetic volcanogenic iron ore deposit in the Western Tianshan Mountains (NW–China): constraints on the age of mineralization and tectonic setting. Gondwana Res. 22, 585–596.
Zhao, J., 2013. Study on the metallogenic settings and metallogenic regularity of copper deposits in western Awulale Mountain, Xinjiang. Ph.D. dissertation of Chang'an University, pp. 1–151.
Zhao, Z., Bai, Z., Xiong, X., Mei, H., Wang, Y., 2003. $^{40}Ar/^{39}Ar$ chronological study of Late Paleozoic volcanic-hypabyssal igneous rocks in western Tianshan, Xinjiang. Geochimica 32, 317–327 (in Chinese with English abstract).
Zhao, X.F., Zhou, M.F., Li, J.W., Wu, F.Y., 2008a. Association of Neoproterozoic A- and I-type granites in South China: implications for generation of A-type granites in a subduction-related environment. Chem. Geol. 257, 1–15.

Zhao, Z.H., Xiong, X.L., Wang, Q., Wyman, D.A., Bao, Z.W., Bai, Z.H., Qiao, Y.L., 2008b. Underplating-related adakites in Xinjiang Tianshan, China. Lithos 102, 374–391.

Zhu, Y., Zhang, L., Gu, L., Guo, X., Zhou, J., 2005. The zircon SHRIMP chronology and trace element geochemistry of the Carboniferous volcanic rocks in western Tianshan Mountains. Chin. Sci. Bull. 50, 2201–2212.

Zhu, Y.F., Zhou, J., Guo, X., 2006a. Petrology and Sr–Nd isotopic geochemistry of the Carboniferous volcanic rocks in the western Tianshan Mountains, NW China. Acta Petrol. Sin. 22, 1341–1350 (in Chinese with English abstract).

Zhu, Y.F., Zhou, J., Song, B., Zhang, L.F., Guo, X., 2006b. Age of the "Dahalajunshan" formation in Xinjiang and its disintegration. Geol. China 33, 487–497 (in Chinese with English abstract).

Zhu, Y.F., Guo, X., Song, B., Zhang, L.F., Gu, L.B., 2009. Petrology, Sr–Nd–Hf isotopic geochemistry and zircon chronology of the Late Palaeozoic volcanic rocks in the southwestern Tianshan Mountains, Xinjiang, NW China. J. Geol. Soc. 166, 1085–1099.

Zhu, Z.M., Zhao, Z.H., Xiong, X.L., Han, J.W., 2010. Petrogeochemistry of Late Paleozoic gabbroic rocks from Tekes County in West Tianshan Mountains. Acta Petrol. Mineral. 29, 675–690 (in Chinese with English abstract).